Central Himalayan rivers record the topographic signature of erosion by glacial lake outburst floods

Maxwell P. Dahlquist[1], A. Joshua West[2]

[1] Department of Earth and Environmental Systems, Sewanee: The University of the South, Sewanee, Tennessee, 37383, USA
[2] Department of Earth Sciences, University of Southern California, Los Angeles, California 90089, USA

Correspondence to: Maxwell P. Dahlquist (mpdahlqu@sewanee.edu)

Abstract. In steep landscapes, river incision sets the pace of landscape evolution. Transport of coarse sediment controls incision by evacuating material delivered to river channels by landslides. However, large landslide-derived boulders that impede bedrock erosion are immobile even in major runoff-driven floods. Glacial lake outburst floods (GLOFs) mobilize these boulders and drive incision, yet their role in regional-scale erosion is poorly understood, largely because of their rarity. Here, we find a topographic signature consistent with widespread GLOF erosion in the Nepal Himalaya. In rivers with glaciated headwaters that generate GLOFs, valleys stay narrow and relatively free of sediment, with bedrock often exposed to erosion. In turn, tributaries to these valleys are steep, allowing less efficient erosional regimes to keep pace with GLOF-driven incision. Where GLOFs are less frequent, valleys are more alluviated and incision stalls. Our results suggest the extent of headwater glaciation may play an important role in erosion of Himalayan river valleys and deserves more attention in future work.

1 Introduction

1.1 Motivation

The erosion of mountainous topography crafts the shape of Earth's surface, influences atmospheric circulation and global climate, modulates global carbon and nutrient fluxes, and affects the tempo of natural hazards including earthquakes and landslides (Raymo and Ruddiman, 1992; Hilton and West, 2020; Steer et al., 2014; Larsen and Montgomery, 2012). At elevations above the equilibrium line altitude (ELA), snow persists from one year to the next, forming glaciers that carve textbook U-shaped valleys (Davis, William Morris, 1900). Fierce debates have centred on the notion that a "glacial erosion buzz-saw" limits the total height and relief of mountain ranges (Brozović et al., 1997; Egholm et al., 2009; Thomson et al., 2010; Cunningham et al., 2019), but even the proponents of this idea generally assume that the influence of glacial erosion fades below the ELA (Prasicek et al., 2018).

Many studies have noted the dramatic erosive power of GLOFs, which arise from the sudden and catastrophic draining of ice or moraine dammed lakes (Mason, Kenneth, 1929; Haeberli, Wilfried, 1983; Montgomery et al., 2004). The resulting floods

Style Definition: Default Paragraph Font

Deleted: (Raymo and Ruddiman, 1992; Hilton and West, 2020; Steer et al., 2014; Larsen and Montgomery, 2012). At elevations above the equilibrium line altitude (ELA), snow persists from one year to the next, forming glaciers that carve textbook U-shaped valleys (Davis, William Morris, 1900). Fierce debates have centred on the notion that a "glacial erosion buzz-saw" limits the total height and relief of mountain ranges (Brozović et al., 1997; Egholm et al., 2009; Thomson et al., 2010; Cunningham et al., 2019), but even the proponents of this idea generally assume that the influence of glacial erosion fades below the ELA (Prasicek et al., 2018).

Deleted: Many studies have noted the dramatic erosive power of GLOFs, which arise from the sudden and catastrophic draining of ice or moraine dammed lakes (Mason, Kenneth, 1929; Haeberli, Wilfried, 1983; Montgomery et al., 2004). The resulting floods can scour river valleys for 10s to 100s of kilometres downstream (Cenderelli and Wohl, 2003; Baynes et al., 2015; Jacquet et al., 2017; Lang et al., 2013; Cook et al., 2018), in some cases mobilizing boulders that otherwise remain stationary even during heavy rainfall-driven flooding (Cook et al., 2018; Xu, 1988). The leading edge of an outburst flood remains below its transport capacity because the velocity of the water bore exceeds that of entrained bedload. Thus, GLOFs remain capable of mobilizing additional material as they progress downstream. These features make GLOFs highly effective incision mechanisms even in low-gradient channels (Cook et al., 2018; Pickering et al., 2019). These events can thus extend the imprint of glacier-associated erosion well below the elevations that support glaciers themselves. ¶
¶
While the dramatic effects of GLOFs have been well-documented, their rarity has made it challenging to identify whether these floods are sufficiently frequent and widespread to play an important role in controlling the long-term evolution of mountain topography. Evidence from glacial lake-derived valley fill and river profiles in the Shyok and Indus valleys suggests that fluvioglacial interactions promote incision into the western edge of the Tibetan Plateau (Scherler et al., 2014).

can scour river valleys for 10s to 100s of kilometres downstream (Cenderelli and Wohl, 2003; Baynes et al., 2015; Jacquet et al., 2017; Lang et al., 2013; Cook et al., 2018), in some cases mobilizing boulders that otherwise remain stationary even during heavy rainfall-driven flooding (Cook et al., 2018; Xu, 1988). The leading edge of an outburst flood remains below its transport capacity because the velocity of the water bore exceeds that of entrained bedload. Mobilization of sediment requires flow to exceed a certain critical shear stress, which is a function of the average particle size and the fluid and sediment densities. The bed shear stress exerted by flow is dependent on the flow depth and velocity, but energy expended by bedload transport decreases the ability of a flood to mobilize new material (Shields, 1936). Since GLOFs maintain a relatively sediment-sparse pulse of water at their front, they remain capable of mobilizing additional material as they progress downstream. These features make GLOFs highly effective incision mechanisms even in low-gradient channels (Cook et al., 2018; Pickering et al., 2019). These events can thus extend the imprint of glacier-associated erosion well below the elevations that support glaciers themselves.

While the dramatic effects of GLOFs have been well-documented, their rarity has made it challenging to identify whether these floods are sufficiently frequent and widespread to play an important role in controlling the long-term evolution of mountain topography. Evidence from glacial lake-derived valley fill and river profiles in the Shyok and Indus valleys suggests that fluvioglacial interactions promote incision into the western edge of the Tibetan Plateau (Scherler et al., 2014). Yet this effect is juxtaposed against the long-term inhibition of erosion as a result of lakes formed by glacial dams (Korup et al., 2010). Here, we evaluate the valley and channel morphology of rivers draining the Nepal Himalaya, finding signatures that are consistent with a systematic role for GLOFs as important agents of long-term erosion. Specifically, we compared rivers that have glaciated (or recently glaciated) headwaters versus those that do not, finding that rivers with glaciated headwaters are distinct both in valley width and channel steepness of tributaries to the main glaciated trunk streams draining the central Himalaya. Furthermore, we observe that knickpoints are concentrated in tributaries more likely to have experienced repeated GLOFs. We attribute these differences to the long-term imprint of repeated GLOFs. Our results suggest "top-down" glacially conditioned erosion may be important across more of the landscape in major mountain ranges than currently recognized, which would have fundamental implications for the coupling of tectonics, erosion, and landscape evolution, and for the interpretation of tectonic processes from river channel form.

1.2 Setting: The role of GLOF erosion in the Nepal Himalaya

The Nepal Himalaya are a leading exemplar of an actively eroding mountain range, offering an ideal environment for investigating the relationships among tectonics, topography, and erosion. The major rivers in Nepal have their headwaters in Tibet and flow across the High Himalaya and Middle Hills, crossing a sharp physiographic transition (PT) as they pass into the lower relief zones of the Himalayan Middle Hills, and then transiting through the Siwalik Hills before ultimately draining onto the Gangetic Plain (Figure 1A). Tributaries to these rivers drain widely varying topography characterized by diverse

Deleted: (Korup et al., 2010).

Deleted: relationships between

Deleted: and

Deleted: driven

Deleted: The Nepal Himalaya are a leading exemplar of an actively eroding mountain range, offering unique opportunities for understanding the relationships between tectonics, topography, and erosion. The major rivers in Nepal have their headwaters in Tibet and flow across the High Himalaya and Middle Hills, ultimately draining onto the Gangetic Plain (Figure 1A). Tributaries to these rivers drain widely varying topography characterized by diverse geomorphic processes (Whipple and Tucker, 1999; Montgomery and Foufoula-Georgiou, 1993). Many of the major rivers have large areas of glaciated headwaters, and much attention has focused on the hazard posed by increasing GLOF frequency in a warming climate (Korup and Tweed, 2007; Veh et al., 2020). Investigation of the role of GLOFs in shaping this landscape remains limited largely to individual case studies (Cenderelli and Wohl, 2003; Cook et al., 2018), along with identifying sedimentary evidence of past GLOF activity (Pickering et al., 2019; Huber et al., 2020). ¶ ... [1]

geomorphic processes (Whipple and Tucker, 1999; Montgomery and Foufoula-Georgiou, 1993). Many of the major rivers have large areas of glaciated headwaters, and much attention has focused on the hazard posed to this region by increasing GLOF frequency in a warming climate (Korup and Tweed, 2007; Veh et al., 2020). Investigation of the role of GLOFs in shaping this landscape remains limited largely to individual case studies (Cenderelli and Wohl, 2003; Cook et al., 2018), along with identifying sedimentary evidence of past GLOF activity (Pickering et al., 2019; Huber et al., 2020).

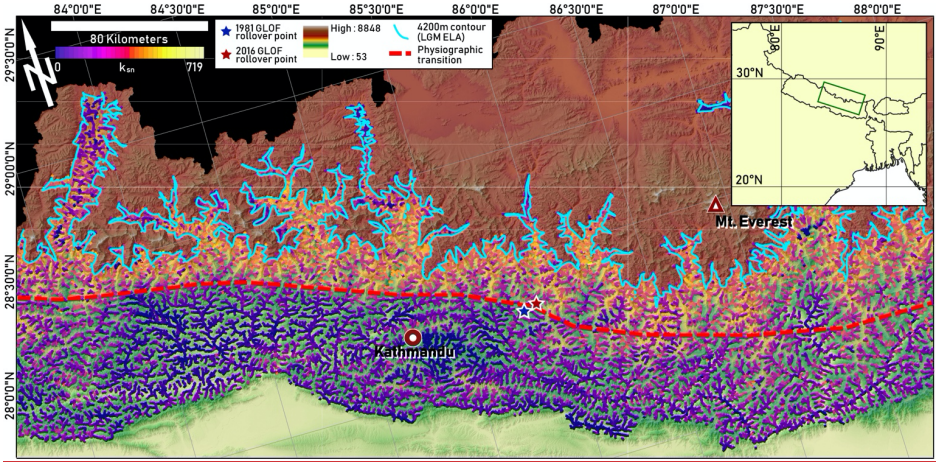

Figure 1 (a) Overview map of the study area, showing equilibrium line altitude at the Last Glacial Maximum (LGM ELA) along with other points of interest. k_{sn} values are overlain on river network for elevations below LGM ELA (Asahi et al., 2010) and were analyzed only where direct glacial action did not appear to be a major erosion mechanism. PT is assessed visually based on abrupt change in relief.

To test for a signature of pervasive GLOF control on erosion across the central Nepal Himalaya, we calculated metrics of river profile morphology, specifically **(1)** normalized channel steepness adjusted for precipitation and evapotranspiration, **(2)** the prevalence of knickpoints in tributary channels, and **(3)** valley width and normalized valley wideness. We interpret the river channel metrics in the context of the upstream drainage area above the last glacial maximum ELA (LGM ELA), estimated to have been 4200 meters in the Nepal Himalaya (Asahi, 2010). We assume that the frequency of GLOFs was proportional to the potentially glaciated terrain in each basin.

We used the LGM ELA on the basis that river morphology expressed today reflects the integration of erosional processes over the several thousand years of glacial retreat (Ray and Srivastava, 2010). There are several important caveats to this assumption.

Deleted: *

Deleted: calculated

Deleted: (b) k_{sn}* ratios at confluences included

Deleted: this study, where Strahler order 1 and 2 tributaries enter order 3 or higher trunk streams. Markers are placed at the confluence where the k_{sn}* ratio was measured.

Deleted: We interpreted the river channel metrics in the context of the upstream drainage area above the last glacial maximum ELA (LGM ELA), estimated to have been 4200 meters in the Nepal Himalaya (Asahi, 2010).

Deleted: We used the LGM ELA on the basis that river morphology expressed today reflects the integration of erosional processes over the several thousand years of glacial retreat (Ray and Srivastava, 2010). While outburst floods originating from landslide-dammed lakes are also common in the Himalaya and are also important geomorphic agents (Hewitt, 1998), we do not expect an obvious relationship between upstream glaciers and landslide-dammed lakes, so our analysis based on drainage area above the LGM ELA limits our focus to GLOF features. The assumption that drainage area above the ELA is proportional to GLOF frequency is imperfect, since, for example, the extent of glaciation on the Tibetan Plateau during the LGM is debated even though this area lies above the ELA (Kirchner et al., 2011). We account for this particular factor by excluding rivers that drain substantial area of the Tibetan Plateau from our analysis. We also reduce the likelihood of region-to-region variability in GLOF frequency affecting our results, by focusing our study area within the Central Himalaya region which is frequently considered as a coherent unit in hazard analyses of GLOFs (Veh et al., 2019; Fischer et al., 2020). In this region, glacier mass balance (which is intrinsically tied to glacial volume) has been found to be related to the frequency of floods originating in moraine-dammed lakes (Fischer et al., 2020). While the relationship between upstream drainage area above the ELA and outburst flood frequency is likely non-linear, we maintain that it is a reasonable proxy for regional-scale assessment. Upstream glaciers also have an important influence on non-outburst flood runoff, contributing meltwater during the hottest months of the summer, generally during the monsoon months. This meltwater can exacerbate monsoon-driven flooding, which does add a complicating factor (Lutz et al., 2014). However, the immobility of large boulders in monsoon-driven floods still points to GLOFs as an important erosional mechanism.

First, outburst floods originating from landslide-dammed lakes are also common in the Himalaya and are also important geomorphic agents (Hewitt, 1998), but we do not expect a straightforward relationship between upstream glaciers and landslide-dammed lakes. So, our analysis based on drainage area above the LGM ELA limits our focus to the particular effect of GLOFs. The stochastic distribution of landslides and landslide dams makes spatial analysis of the topographic effect of landslide lake outburst floods more difficult, though an interesting problem for future work. Second, the assumption that drainage area above the ELA is proportional to GLOF frequency is imperfect, since, for example, the extent of glaciation on the Tibetan Plateau during the LGM is debated even though this area lies above the ELA (Kirchner et al., 2011). Third, factors such as valley geometry, glacial dynamics, and seismicity also play roles in GLOF generation, though evaluating these factors is beyond the scope of this study. Fourth, upstream glaciers also have an important influence on non-outburst flood runoff, contributing meltwater during the hottest months of the summer, generally during the monsoon months. This meltwater can exacerbate monsoon-driven flooding even in the absence of GLOF generation (Lutz et al., 2014).We reduced the likelihood of region-to-region variability in GLOF frequency affecting our results by focusing our study area within the Central Himalaya region which is frequently considered as a coherent unit in hazard analyses of GLOFs (Veh et al., 2019; Fischer et al., 2021). In this region, total glacier mass balance, i.e. the regional difference between ice accumulation and meltoff (which is intrinsically tied to glacial volume), has been found to be related to the frequency of floods originating in moraine-dammed lakes (Fischer et al., 2021). The relationship between upstream drainage area above the ELA and outburst flood frequency is likely non-linear, but we maintain that it is a reasonable proxy for regional-scale assessment. Despite the many complicating variables at play which we do not attempt to entirely account for, here, we will test the hypothesis that the immobility of large boulders in monsoon-driven floods points to GLOFs as an important erosional mechanism. To do this, we present a conceptual model for a potential river morphologic response if repeated GLOFs are indeed effective enough as geomorphic agents to leave topographic evidence in the regional landscape. We then test this model against several lines of topographic evidence found in the Himalayan landscape.

1.3 Conceptual model for river morphologic response to GLOF erosion

At elevations below the extent of glaciation, rivers are the main pacemakers of erosion. The erosive power of rivers is controlled by their base level, which is the lowest elevation of active fluvial erosion. Base level is scale-dependent, and might be defined for a tributary as the elevation of the junction with a higher-order stream, affected by incision and aggradation in the trunk stream. Regionally, it might be the defined by elevation of an alluvial fan at a range front, while globally, base level is sea level. Uplift of mountainous terrain effectively decreases regional base level, driving rivers to steepen and incise more deeply into uplifting rock. This incision steepens surrounding hillslopes, which respond by eroding faster (Burbank et al., 2003). According to the detachment-limited framework for river evolution, fluvial erosion is driven "from the bottom up," whereby base level change begins at low elevations (e.g., at river outlets) and moves upstream from there, producing a wave of incision and hillslope lowering that works its way through the landscape (Figure 2A-C) (Howard, 1994).

Deleted: Uplift of mountainous terrain effectively decreases

Deleted: (Burbank et al., 2003).

Deleted: (Howard, 1994).

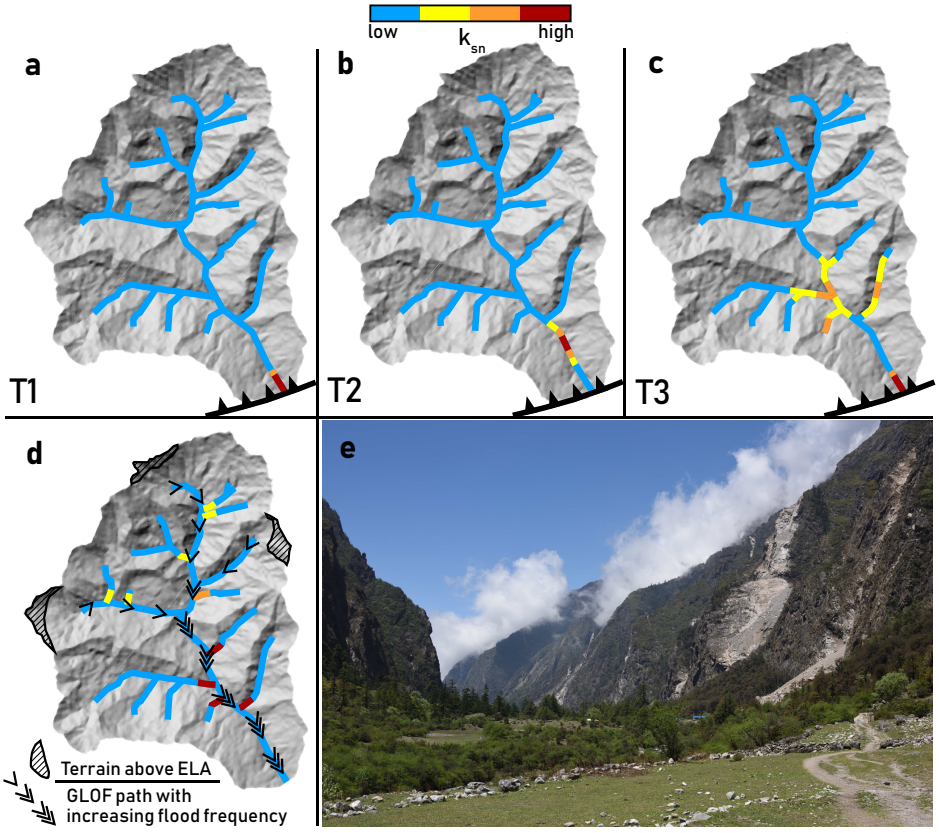

235

Figure 2 (a) Schematic of predicted k_{sn} patterns arising from erosion driven by upstream knickpoint migration resulting from base level fall, including knickpoint diffusion described in alluvial and bedrock-alluvial channels (Rosenbloom and Anderson, 1994). (a-c) represent time steps showing the evolution of k_{sn} patterns following a base level fall initiating at the thrust fault at the outlet of the catchment (panels A-C reflect temporal progression). In 1c, a second base level fall has initiated. (d) Schematic of k_{sn} patterns we hypothesize to arise from erosion driven by GLOFs originating from the high-elevation regions shown as terrain above ELA. Steepened reaches formed near confluences may migrate upstream, steepening the basin at large. Our aim

240

Deleted: T1 to T3 reflects

Deleted: steady state

in illustrating the simple scenario shown in panels a-c is not to suggest it as a plausible representation of the tectonic geomorphology of the Himalaya, but instead to contrast the end-member expectations from erosion purely driven by changes in base level versus the conceptual model we propose for glacial lake outburst flood (GLOF)-driven erosion, in panel d — while recognizing that actual erosion in Himalayan river valleys will involve a collaboration between these end-member scenarios. (e) Photograph from Langtang Valley, Nepal, showing steep inner valley walls and steep tributary catchments entering the trunk valley ~1 kilometer below the lowest identified glacial surfaces. Photo location is 28.200° N, 85.460° E.

This simple conceptual model finds natural expression in fault-block mountains where uplift is focused on a single fault at the base of the range (Whittaker, 2012). In such settings and under the right conditions, the topographic profiles of rivers preserve quantitative information about the tectonic and geodynamic drivers of uplift, or about past change in climate (Whipple and Tucker, 1999). In more complex mountain ranges, numerous other processes can affect river incision and erosion, including differential rock uplift associated with multiple active tectonic features (Kirby and Whipple, 2001), gradients in precipitation and channel width (Roe et al., 2003; Finnegan et al., 2005), and variations in lithology, rock strength, and sediment availability (Sklar and Dietrich, 2001, 2006). In addition, high-magnitude, infrequent events, such as GLOFs, play key roles in erosion (Kirchner et al., 2001; Cook et al., 2018) -- yet their role in modulating the response of incision to uplift is poorly understood.

1.4 Morphometric proxies of GLOF erosion

We test for three predicted effects of GLOF-driven erosion on the topographic form of rivers in the central Himalaya. The first of these is the steepness of river channels. Normalized channel steepness (k_{sn}) represents the steepness of channels after accounting for the typically concave form of most river profiles. This concave form is reflected in a power law relationship between channel slope (S) and upstream area (A), where

$$S = k_{sn} A^{-\theta} \quad (1)$$

If θ is fixed to a best-fit reference value, the normalized channel steepness k_{sn} provides a basis for comparing the relative steepness of different channels (see Methods) (Flint, 1974). Differences in k_{sn} between river segments have been attributed to variations in uplift (faster uplift requires a steeper, more energetic river for incision to keep pace), local rock strength (stronger rocks require more energy to erode), sediment supply (competing effects of tools and cover either enhance or inhibit erosion), and climate (less discharge means less erosive power, requiring steeper channels). Importantly for our purposes, GLOFs may influence k_{sn} because they are highly effective erosional agents, capable of exerting extreme bed shear stresses by the progress of a high-velocity pulse of water even in a low-gradient river. High-magnitude, low-frequency discharge events, of which lake outburst floods are the apotheosis, are recognized as a critical control on erosion and on the geometry of channels, particularly where discharge thresholds for initiation of erosion are high (Snyder et al., 2003; Lague et al., 2005; Turowski et al., 2009; DiBiase and Whipple, 2011). As a result, erosional efficiency can be enhanced under conditions where channel steepness is low, mean discharge and discharge variability are high, and incision thresholds are high (DiBiase and Whipple, 2011). The

Deleted: an

Deleted: This simple conceptual model finds natural expression in fault-block mountains where uplift is focused on a single fault at the base of the range (Whittaker, 2012). In such settings and under the right conditions, the topographic profiles of rivers preserve quantitative information about the tectonic and geodynamic drivers of uplift, or about past change in climate (Whipple and Tucker, 1999). In more complex mountain ranges, numerous other processes can affect river incision and erosion, including differential rock uplift associated with multiple active tectonic features (Kirby and Whipple, 2001), gradients in precipitation and channel width (Roe et al., 2003; Finnegan et al., 2005), and variations in lithology, rock strength, and sediment availability (Sklar and Dietrich, 2001, 2006). In addition, extreme, infrequent events (such as GLOFs) play key roles in erosion (Kirchner et al., 2001; Cook et al., 2018), yet their role in modulating the response of incision to uplift is poorly understood.¶

Deleted: $S = k_{sn} A^{-\theta}$

Deleted: (Flint, 1974).

Deleted: (Snyder et al., 2003; Lague et al., 2005; Turowski et al., 2009; DiBiase and Whipple, 2011).

Deleted: (DiBiase and Whipple, 2011).

major rivers of the Nepal Himalaya should meet these conditions, with discharge peaks defined by catastrophic outburst floods and incision thresholds governed by the presence of ~10 meter-scale boulders in the channel. We thus expect river segments that are influenced by GLOFs to erode more rapidly than rivers with similar geometry and characteristic grain size and lithology without GLOFs. Therefore, we expect that GLOF-influenced rivers will drive their non-GLOF influenced tributaries toward higher k_{sn} for the same erosion rate than if runoff-driven floods were the dominant erosional mechanism. If correct, this effect should be detectable in the geometry of tributary channels (Figure 2D).

Secondly and similarly, we expect GLOF erosion may be associated with discrete steepened reaches (knickpoints) in tributary channels near their outlets into larger trunk streams. In our proposed model for GLOF erosion, knickpoints should form in tributaries as a result of pulses of GLOF incision in the trunk stream. A concentration of knickpoints near trunk streams where outburst floods are more frequent would support an erosion model where GLOFs are an important factor. This is not to suggest that outburst floods are the only means by which knickpoints can develop at confluences. Punctuated incision, which may result in steepened reaches developing in tributaries, has been documented at a variety of timescales in rivers with different characteristics, and knickpoints generated at regional base level may propagate upstream and stall at confluences (Gardner et al., 1987; Crosby and Whipple, 2006; Finnegan et al., 2014). However, we hypothesize that outburst flood-driven incision may be particularly effective at generating knickpoints at tributary junctions due to the magnitude of erosion that may occur in a single event, particularly for rivers where GLOFs are relatively frequent.

Thirdly, the removal of coarse sediment by GLOFs is expected to change river valley widths. We propose that outburst floods facilitate river incision by mobilizing very coarse sediment, including large boulders, that remains stationary even during large runoff-driven floods. The widths of valley floors should reflect the degree of aggradation at longer timescales than the width of the active channels (Schwanghart et al., 2016; Yanites et al., 2018). If floods clear out aggraded material, we expect to see a narrowing trend in rivers subject to more GLOF activity if our erosion model depicted in Figure 2d plays a substantial role in Himalayan river incision. To test this prediction, we analysed valley floor widths based on a discharge-adjusted normalized channel wideness index (k_{wn}^*, see Methods) to account for the typical power-law increase in valley width with discharge.

2 Methods

We evaluated the metrics described above for a region of central Nepal characterized by N-S trending rivers draining across the Himalayan range (Figure 1). These rivers differ significantly in the extent of upstream glaciated area at the LGM. To complete topographic analysis of this region, we used the Shuttle Radar Topography Mission (SRTM) 30-meter digital elevation model (DEM), patched with the Advanced Spaceborne Thermal Emission and Reflection Radiometer (ASTER) 30-meter DEM where voids exist in SRTM. For the knickpoint analysis, we supplemented the 30m SRTM DEM with the 10m-

Deleted: , all other factors being equal, and therefore
Deleted: require lower
Deleted: the
Deleted: (Gardner et al., 1987; Finnegan et al., 2014).
Deleted: tributaries
Deleted: (Schwanghart et al., 2016; Yanites et al., 2018).
Deleted: 2D
Deleted: of
Deleted: Materials and

resolution EarthDEM (Polar Geospatial Center, 2021). Since we are not concerned with resolving small-scale features in our k_{sn} analysis and the EarthDEM contains more voids and artifacts than the SRTM, we determined that the lower resolution DEM was more appropriate for k_{sn} applications. Topographic metrics were calculated using the TopoToolbox and Topographic Analysis Kit packages for Matlab, and the DEM was preprocessed to remove outliers and impose a minimum downstream gradient for analysis of channel profiles (Forte and Whipple, 2019; Schwanghart and Scherler, 2014). In this section, we provide further detail on the determination of these metrics.

Deleted: (Forte and Whipple, 2019; Schwanghart and Scherler, 2014).

2.1 Physical Relationships in Channel Networks

In actively uplifting landscapes, the geometry of the land surface is governed by competition between uplift and gravity, mediated by a series of processes with a variety of controlling factors. In time, this competition tends to result in a time-invariant condition of topographic steady state (Whipple and Tucker, 1999; Willett and Brandon, 2002). For most of the Earth's surface, local boundary conditions for erosion are set by the pace of incision or aggradation associated with river channel processes. In channel networks, the relationship between channel slope and contributing drainage area can reveal the active erosional processes. Downstream reaches of the channel network, which are typically controlled by fluvial processes, are described by the power law function

Deleted: stalemate, a time-invariant condition of topographic steady state (Whipple and Tucker, 1999; Willett and Brandon, 2002).

$$E = KA^m S^n \quad (2)$$

where E is erosion rate, K is the erosion coefficient, which is governed by local lithology, climate, and the process that control incision in the area, A is drainage area, S is local slope, and m and n are empirical constants which have a range of possible values depending on local conditions. Under steady-state conditions, where uplift and erosion can be assumed to be equal,

$$S = \left(\frac{U}{K}\right)^{\frac{1}{n}} A^{\frac{m}{n}} \quad (3)$$

where U is uplift (Whipple and Tucker, 1999). This equation can be recast as Equation 1, known as Flint's Law, where k_s defines a channel steepness $\left(\frac{U}{K}\right)^{\frac{1}{n}}$. The parameter θ, termed the concavity, which under conditions of spatially invariant uplift and erodibility equals m/n, represents the rate of change of channel slope with drainage area and is generally accepted to be insensitive to uplift rate (Flint, 1974). k_s varies with uplift rate but contains units that are dependent on θ. In order to make a reasonable comparison of k_s among channels with different θ, we must fix the value of θ to a reference concavity, θ_{ref}, that represents an average value for the channels in the area of interest, typically between 0.35-0.65, although this value may vary widely depending on local factors (Wobus et al., 2006a).

Deleted: where U is uplift (Whipple and Tucker, 1999). This equation can be recast as Equation 1, known as Flint's Law, where k_s defines a channel steepness $\left(\frac{U}{K}\right)^{\frac{1}{n}}$. The parameter θ, termed the concavity, which under conditions of spatially invariant uplift and erodibility equals m/n, represents the rate of change of channel slope with drainage area and is generally accepted to be insensitive to uplift rate (Flint, 1974). k_s varies with uplift rate but contains units that are dependent on θ. In order to make a reasonable comparison of k_s among channels with different θ, we must fix the value of θ to a reference concavity, θ_{ref}, that represents an average value for the channels in the area of interest, typically between 0.35-0.65, although this value may vary widely depending on local factors (Wobus et al., 2006a).¶

2.2 Normalized channel steepness index (k_{sn})

Fixing θ to θ_{ref} results in the normalized channel steepness index k_{sn} which is calculated as a best fit value for a given channel reach and is frequently and effectively used as a proxy in broad comparisons of uplift and incision rates across landscapes (Wobus et al., 2006a). Equation 3 is recast as

$$S = k_{sn} A^{-\theta_{ref}} \quad (4)$$

We found a best-fit θ_{ref} of 0.3513 and used this value for all k_{sn} calculations in this study. We used the Topographic Analysis Kit to calculate k_{sn} using the "KsnChiBatch" function, which fits k_{sn} for channel network segments using desired criteria (Forte and Whipple, 2019). To examine the tributary basin response to GLOF erosion in the trunk streams, we used basin-averaged k_{sn} in our analyses. Equations 3 and 4 are derived from the detachment-limited stream power model (Howard, 1994), and a comparison of k_{sn} among channels assume that all erode accordingly. To exclude channels that do not behave according to the detachment-limited stream power model, we set a minimum drainage area to define a stream as 2 km^2 to avoid most channels where debris flow action is the main erosion mechanism. We have also excluded tributaries where the trunk valley at the confluence point has geometry that is indicative of erosion by direct glacial action (U-shaped valleys), tributaries where the tributary basin was likely to have been glaciated in its headwaters at the LGM (and thus may have experienced GLOF erosion as well). We have included tributaries where the trunk channel has extensive headwaters on the Tibetan Plateau (data points above 10^{10} m^2 on Figure 3), although the extent of glaciation on the Tibetan Plateau is still debated and a wide range of possibilities may be realistic (Kirchner et al., 2011). If regions above 4200 meters on the plateau were potentially ice-free at the LGM, then our proxy for GLOF frequency (total drainage area above the LGM ELA) may not apply in these rivers. However, as those channels do not deviate from the overall trends we identified, we found it appropriate to include them.

2.3 Knickpoint Distribution

For our analysis of knickpoint distribution, we used the "knickpointfinder" function in TopoToolbox to identify and inventory knickpoints in the study area (Schwanghart and Scherler, 2014, Supplemental Figure S1). To reliably identify knickpoints which might be missed in the 30-meter SRTM DEM, we obtained the EarthDEM 10-meter DEM, which is itself downsampled from a 2-meter DEM derived from stereo pairs of optical satellite imagery (Polar Geospatial Center, 2021). Tributaries included in the knickpoeint inventory are 1st-3rd order streams that drain into 4th or higher order trunk streams (see example river profiles in Supplemental Figure 2). Similar to our k_{sn} analysis, we excluded tributaries to trunk streams that substantially drain the Tibetan Plateau since the extent of LGM glaciation on the plateau is much debated. We set a minimum relief of 20 meters as the threshold for inclusion, to minimize the possibility of false knickpoints arising from noise in the topographic data. Since knickpoints can arise from many different geologic processes, we conducted the knickpoint search on parts of the tributary network we assume to be most affected by potential geologically recent outburst floods in the trunk channel, within 2 kilometres of a trunk stream. We included all tributaries below the region we expect to

Deleted: .2 Adjusted normalized

Deleted: *)

Deleted: Fixing θ to θ_{ref} results in the normalized channel steepness index k_{sn} which is calculated as a best fit value for a given channel reach and is frequently and effectively used as a proxy in broad comparisons of uplift and incision rates across landscapes (Wobus et al., 2006a). However, a key feature of Equation 1 is that drainage area A is used as a proxy for water discharge Q, which is the parameter presumed to drive incision. In general, larger drainage areas produce higher discharge, so that A can be assumed directly proportional to Q. However, given the dramatic gradient in precipitation from the Gangetic Plain to the Tibetan Plateau, contributing drainage area on its own is not an accurate proxy for discharge in this setting. We used a modified metric, k_{sn}^*, which accounts for variation in runoff across the region, since runoff may substantially affect k_{sn} (Gasparini and Whipple, 2014). To calculate k_{sn}^*, we estimated the contributing runoff from each DEM grid cell using mean annual precipitation (P) from a 12-year (1998-2009) Tropical Rainfall Measuring Mission (TRMM) dataset (Bookhagen, 2013) and evapotranspiration (ET) from the Global Land Evaporation Amsterdam Model (GLEAM) (Martens et al., 2017) and used the resulting runoff estimate to weight cells when calculating contributing drainage area. ↵
We recast Equation 3 as →¶
$S = k_{sn}^* Q^{-\theta_{ref}^*}$ →→→→→→→→→→→→→→ (4)↵
with Q representing estimated discharge from the water balance (P – ET) in each DEM cell. This approach ignores any spatial variation in water storage, which we expect to be small. →↵
↵
Employing our discharge estimate and plotting slope against discharge for all channels across our study area`, we found a best-fit θ_{ref}^* of 0.0781 and used this value for all k_{sn}^* calculations in this study. We used the Topographic Analysis Kit to calculate k_{sn}^* using the "trib" method, which fits k_{sn}^* for channel network segments between confluences individually, calculating tributaries separately from trunk streams for the most accurate representation of k_{sn}^* patterns near confluences (Forte and Whipple, 2019). To compare tributary and trunk stream k_{sn}^*, we take the k_{sn}^* value for the tributary at the channel node closest to 200 meters from the confluence (Figure 1B). Given the resolution of the DEM (30 meter grid spacing) and possible orientations of channel nodes, this will be 5-7 nodes from the confluence. We use the k_{sn}^* value 200 meters from the confluence to avoid taking tributary k_{sn}^* values from stream segments that are in the valley bottom of the trunk stream. We set a minimum drainage area to define a stream as 0.48 km^2 following Roback et al. (Roback et al., 2018). In our k_{sn}^* ratio analysis, we have excluded confluences where the trunk valley at the confluence point has geometry that is indicative of erosion by direct glacial action (U-shaped valleys), confluences where the tributary channel was likely to have been glaciated in its headwaters at the LGM (and thus may have experienced GLOF erosion as well), and confluences where the trunk channel has extensive headwaters on the Tibetan Plateau. We excluded the last category because the extent of glaciation on the Tibetan Plateau is still debated and a wide r ... [2]

Deleted: (Schwanghart and Scherler, 2014). Tributaries included in the knickpoint inventory are 1st or 2nd order streams that drain into 4th or higher order trunk streams and are at least 690 meters ASL (see example river profiles in Supplement Figure 2). Similar to our k_{sn}* ratio

Deleted: confluences between

have been modified directly by glacial erosion in the knickpoint search and binned them against upstream drainage area above the LGM ELA in the trunk stream. We also examined the knickpoints identified by the function to ensure that the vast majority of them represent bedrock features, rather than incision into valley fill (Figure S3).

2.3 Normalized channel wideness index (k_{wn})

Most fluvial networks are characterized by a power-law increase in the width of channels as a function of contributing drainage area (Leopold and Maddock, 1953). This relationship is governed by many factors, including erosion rate, lithology, and climate, among others. Particularly in regions where extreme events can generate massive sediment inputs, channel width increases with aggradation (Schwanghart et al., 2016). Unit stream power is greater where channels are narrower, so channels may narrow to more readily expose bedrock and facilitate incision (Croissant et al., 2017). Dynamic channel width may thus illustrate channel response to tectonic or process-driven forcing. Channel width follows a power law relationship with discharge (Leopold and Maddock, 1953), as

$$W = k_w Q^b \quad (5)$$

where W is the channel width, k_w is a channel wideness index analogous to k_s, while Q represents (in our case, estimated) discharge from the water balance (P – ET) in each DEM cell. This approach ignores any spatial variation in water storage, which we expect to be small. By fixing a best-fit reference value for b, we can examine local variation in channel wideness in response to enhanced erosion by increased GLOF activity (Allen et al., 2013; Yanites, 2018), using

$$W = k_{wn} \quad Q^{b_{ref}} \quad (6)$$

To calculate Q, we estimated the contributing runoff from each DEM grid cell using mean annual precipitation (P) from a 12-year (1998-2009) Tropical Rainfall Measuring Mission (TRMM) dataset (Bookhagen, 2013) and evapotranspiration (ET) from the Global Land Evaporation Amsterdam Model (GLEAM) (Martens et al., 2017) and used the resulting runoff estimate to weight cells when calculating contributing drainage area.

To investigate the influence of GLOFs on channel width patterns, we used Google Earth imagery to make 1,598 width measurements from rivers across our study area, spacing measurements roughly equally along river reaches (Supplemental Figure S1). We measured the widths of valley bottoms instead of the channels themselves, since the active channel can change in width rapidly with deposition from local landslides and subsequent evacuation of deposits. Since glaciers can extend far below the ELA and we aim to avoid analyzing valleys subject to direct ice action, we avoided taking width measurements at elevations above 3,000 meters except in a few locations where a V-shaped valley profile was very well-developed. We determined the location of transitions from valley floors to hillslopes by observations of several features. Many valley bottoms

Deleted: trunk streams from which
Deleted: is reported.
Deleted: Adjusted normalized
Deleted: *)
Deleted: .
Deleted: (Schwanghart et al., 2016) while relative channel width decreases with increased unit
Deleted: ,
Deleted: bedrock is readily exposed and
Deleted: incise downward (Croissant et al., 2017).
Deleted: We can approach
Deleted: width-area trend using an equation with the same form as slope-area, although the
Deleted: between upstream drainage area and width is positive, so
Deleted: A^b(5)
or considering a discharge estimate accounting for precipitation and evapotranspiration in place of drainage area,
$W = k_w{}^* Q^{b^*}$ (6
Deleted: .
Deleted: .
Deleted: 1

have riparian vegetation that is visually distinct from vegetation on the hillslopes. In parts of the study area where valleys and hillslopes are developed for agriculture, farm terraces rapidly narrow where the hillslopes begin to steepen, offering a simple visual indication of the base of the hillslopes. Fluvial terraces are visible in satellite imagery and aid in distinguishing active valley bottom from abandoned surfaces. We included terraces within ~10m of the elevation of the active channel in the valley bottom measurements, since a single outburst flood may incise enough to remobilize terrace material several meters above the active channel (Cook et al., 2018). Our assumption that the width of valley bottoms is analogous to the width of active channels is supported by the observed power law relationships between discharge and valley width in the field area. While the width of the active channel itself can vary significantly over a short time, we expect that, although individual large landslides or other events might cause localized aggradation, on aggregate over our study area the width of the valley floor should reflect longer-term trends given that the timescales inherent in significantly raising or lowering an entire valley floor (and thus widening or narrowing it) should be orders of magnitude longer than timescales governing the width of the channel (Ray and Srivastava, 2010).

2.4 Statistical Analyses

We calculated Spearman rank correlation coefficients (Spearman's ρ) and P-values using the Matlab "corr" function with the "Spearman" parameter. The Spearman's ρ is a nonparametric measure of the strength of association between two variables, specifically useful for testing for a monotonic relationship where the nature of that relationship is unknown (Spearman, 1987). ρ is reported as a value between 1 and -1 indicating the strength of the positive or negative correlation. We chose the Spearman's test since it was unclear what functional form the expected relationships among our variables should take. We also used two-sample Kolmogorov-Smirnov (K-S) tests, which compare the empirical distribution functions of two samples (Massey, 1951). K-S tests were conducted and P-values calculated using the Matlab "kstest2" function. The piecewise polynomial smoothing spline shown in Figure 3 used to determine expected k_{sn} at a given elevation was fit using the Matlab "cftool" utility in the Curve Fitting Toolbox, with smoothing parameter p = 4.4773e^{-09}. We chose a spline fit as the relationship between elevation and k_{sn} appears to be naturally piecemeal, with average k_{sn} increasing nonlinearly with basin elevation until ~2500 meters, at which point it begins to decrease.

3 Results

3.1 GLOFs and Normalized Channel Steepness

Along the course of the major Himalayan rivers, the mainstems typically drain glaciated areas, while many of the tributaries do not. We examined the relationship between channel steepness and potential glacial outburst flooding by calculating the average k_{sn} in tributary basins which drain to rivers with upstream glaciers, specifically in cases where the tributaries themselves are unglaciated (Figure 1). If GLOFs are indeed a regionally important erosional agent, we expect that effective

Deleted: also

Deleted: (Cook et al., 2018).

Deleted: ¶
¶

Deleted: (Ray and Srivastava, 2010). As in our k_{sn}^* calculation, we use TRMM precipitation and GLEAM evapotranspiration data to estimate discharge, calculating a normalized channel wideness index as →
$W = k_{wn}{}^* Q^{b_{ref}{}^*}$ (7)
(Allen et al., 2013; Yanites, 2018).

Deleted: were calculated

Deleted: (Spearman, 1987).

Deleted: (Massey, 1951). K-S tests were conducted and P-values calculated using the Matlab "kstest2" function

Deleted: Ratios Between Tributaries and Trunk Streams

Deleted: compared

Deleted: between these

Deleted: ratio of

Deleted: k_{sn}^* (adjusted

GLOF-driven erosion in trunk streams should drive a topographic response in their tributary basins, which do not have access to highly efficient GLOF erosion. Since k_{sn} is strongly correlated with elevation in the Himalaya, we have accounted for the overall trend between elevation and average k_{sn} and analysed basin averaged k_{sn} in the context of deviation from the expected value at a basin's elevation. Overall, we find that rivers with a greater proportion of upstream glaciated terrain tend to have tributary basins that are generally steeper (Figure 3). We interpret this steepening of tributaries as being a response to accelerated incision rates in the trunk streams driven by GLOFs. Repeated GLOFs occurring from the same source areas along the same flow paths will produce a persistent difference in erosion rate between erosionally less efficient tributaries and GLOF-dominated trunk streams. This difference would require the tributaries that lack glaciated terrain to steepen to keep pace with erosion of the mainstem, leading tributaries to steepen (Figure 2D) — as we observe.

Deleted: accounting

Deleted: variability in discharge; see Materials and Methods) to trunk stream…

Deleted: * near where each tributary joins the mainstem (Figure 1B). Typically, unless a confluence coincides with the location of a lithologic contact, active deformation structure, or transient knickpoint,…

Deleted: * values in

Deleted: mainstem and its tributary measured very close to the confluence should be approximately equal. In many cases

Deleted: tributaries

Deleted: near confluences

Deleted: increasing the k_{sn}^* ratio

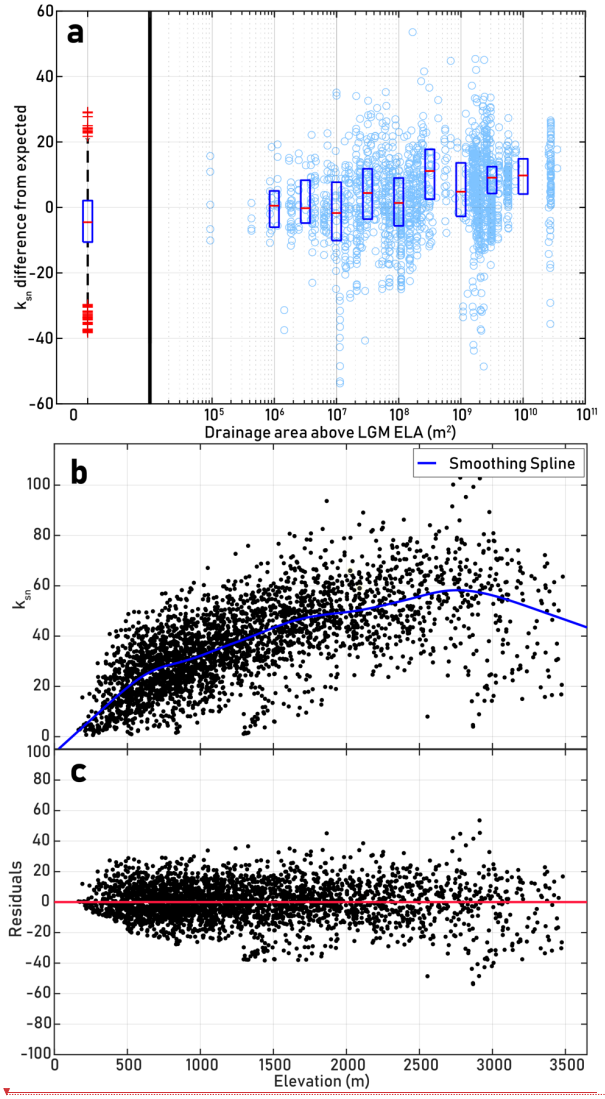
a
b
c
k_{sn} difference from expected
Drainage area above LGM ELA (m²)
Smoothing Spline
k_{sn}
Residuals
Elevation (m)

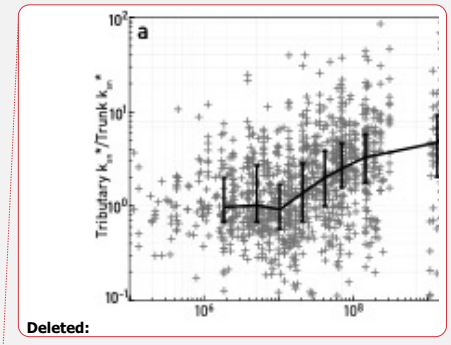
a
Tributary k_{sn}*/Trunk k_{sn}*

Deleted:

Figure 3 (a) Difference between tributary basin average k_{sn} and expected k_{sn} given basin elevation (based on residuals for spline fit shown in Figure 3b-c) versus total drainage area above LGM ELA in trunk stream basin (n = 3047). Box and whisker plot to the left of the break shows distribution of k_{sn} differences for tributaries draining to rivers with no drainage area above 4200 meters. Box shows mean and upper and lower quartiles, whiskers represent 5th and 95th percentiles. Box plots to the right of the break show the mean and upper and lower quartiles for bins centered at boxes. Spearman's rank correlation coefficient (Spearman's ρ), which tests for a potentially nonlinear monotonic relationship, is ρ = 0.3899 with $P < 0.0001$, indicating a statistically significant positive correlation. We conducted a two-sample Kolmogorov-Smirnov test for the distributions of average tributary k_{sn} of basins draining to channels with above-ELA drainage areas between 10^7-10^9 m^2 (n = 754) and 10^9-10^{10} m^2 (n = 748) to determine if the samples come from significantly different distributions, and found the empirical CDF for the first group is larger with $P < 0.0001$. (b) Smoothing spline fit for tributary basin average k_{sn} vs. basin average elevation, calculated using the "cftool" utility from the Matlab Curve Fitting Toolbox. (c) Residuals for smoothing spline fit.

One potential complication is that in small, very steep catchments, such as some of the tributaries examined in this study, debris flows can control channel geometry at drainage areas of up to several square kilometres (Dahlquist and West, 2019). Since channels incising due to debris flow action do not follow a power law relationship between slope and drainage area, the use of k_{sn} as a simple uplift-incision proxy in these catchments is problematic (Stock and Dietrich, 2006). If debris flow erosion is indeed an important control on channel geometry along some of the 1st and 2nd order basins we studied, the steepening trend we observe in tributaries responding to more frequent GLOFs in the trunk channel may reflect steeper tributaries allowing for more frequent debris flows with longer runouts capable of doing more erosional work (Stock and Dietrich, 2006). Yet we argue that this additional erosional work still reflects steepness produced by incision of the main stem, i.e., via GLOF activity.

3.2 Knickpoint distribution and GLOF erosion

To verify whether patterns of knickpoints are consistent with GLOF incision being a prominent component of Himalayan erosion, we analysed the distribution of knickpoints on tributaries within 2 kilometres of 4th or higher order rivers (Supplemental Figure 1, Figure 4). In 3557 tributary channels, we found 3707 knickpoints with at least 20 meters of relief based on the 10m-resolution EarthDEM. We log-binned knickpoint counts and total knickpoint relief by the amount of upstream drainage area above the ELA in the trunk stream that each tributary joins. We then assessed the proportion of knickpoints that are found in tributaries to rivers without glaciated headwaters, and we compared this proportion to that of tributary confluences in general. We found that knickpoints are less common in tributaries to rivers with no glaciated drainage area upstream (Figure 4). Only ~37% of the knickpoints are found on tributaries to rivers without glaciated headwaters; in comparison, 51% of the tributaries analysed drain to rivers with no drainage area above the ELA. This effect is more pronounced when knickpoints are weighted by relief, with only ~33% of the total knickpoint relief found on these tributaries to unglaciated rivers. In tributaries to rivers with substantially glaciated headwaters (draining at least 10 km^2

Deleted: k_{sn}^* ratios
Deleted: tributaries
Deleted: trunk streams measured at confluences
Deleted: upstream
Deleted: the
Deleted: the
Deleted: . Bin centers are median values, edges are
Deleted: . (b) k_{sn}^* ratios at confluences separated into those above and below 690 meters,
Deleted: elevation of the 1981 Bhote Koshi outburst flood discharge rollover point. We use 690 meters as an approximate elevation of …
Deleted: PT in major river channels, to test for the influence of GLOF erosion on valley geometry above vs. below the PT
Deleted: for data above 690 meters
Deleted: 441
Deleted: . We also
Deleted: k_{sn}^* ratios
Deleted: 10^8
Deleted: 488
Deleted: 155
Deleted: many
Deleted: (Dahlquist and West, 2019).
Deleted: * as a simple uplift-incision proxy in these catchments is problematic (Stock and Dietrich, 2006).
Deleted: (Stock and Dietrich, 2006).
Deleted: 3062
Deleted: 5970
Deleted: much
Deleted: 18
Deleted: 30
Deleted: 15
Deleted: rivers,

above 4200 meters) we find over-representation of the knickpoints, with ~50% of knickpoints on these tributaries despite them making up only ~41% of the analyzed rivers. Again, this effect is accentuated when knickpoints are weighted by relief, with these knickpoints on tributaries to glaciated rivers representing ~54% of the total knickpoint relief (Figure 4B).

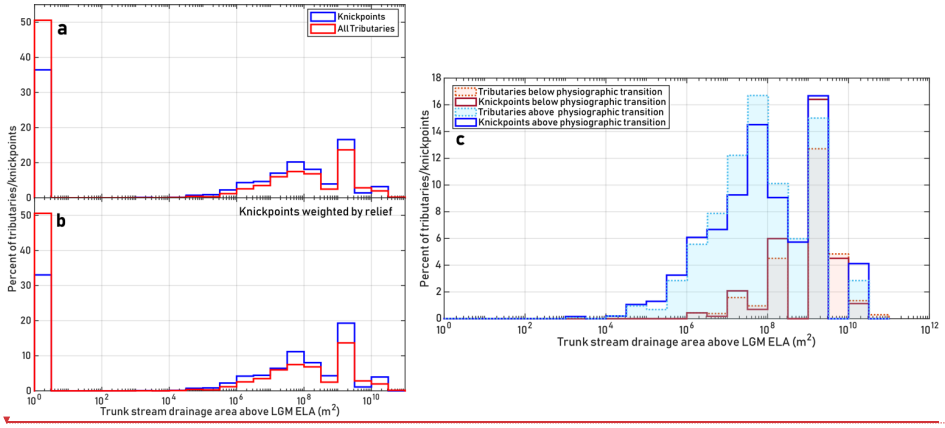

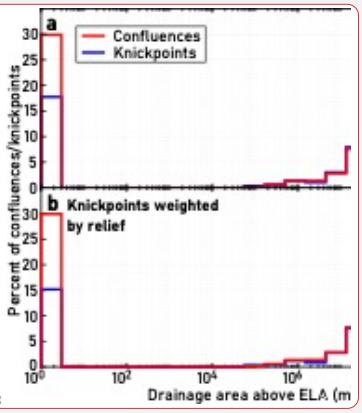

Figure 4 (a) Distribution of knickpoints (n = 3707) and analyzed 1st and 2nd order tributaries (n = 3557) to 3rd or higher order rivers with respect to the area of terrain above the ELA drained by the trunk stream. Knickpoints included in the analysis are located on a 1st or 2nd order tributary within 2 km of a confluence with a 3rd or higher order trunk stream. Area is log-binned, the lowest area bin contains only knickpoints and confluences where the trunk stream does not drain any terrain above the ELA. See Methods for criteria for identifying knickpoints. (b) Same as 4A, but knickpoints are weighted by their relief. For both the relief-weighted and non-weighted knickpoint distributions, we conducted two-sample Kolmogorov-Smirnov tests for the distributions of knickpoints versus confluences with respect to above-ELA drainage areas and found the empirical CDF for the confluences is larger with $P < 0.0001$. (c) Comparison of knickpoints and tributaries located above (n = 1472 tributaries, n = 2549 knickpoints and below (n = 2085 tributaries, n = 1152 knickpoints) the physiographic transition (PT) (Figure 1). Including only those knickpoints and tributaries that drained to trunk streams with drainage area above the LGM ELA, we conducted two-sample Kolmogorov-Smirnov tests for the distributions of knickpoints versus confluences with respect to above-ELA drainage area, and found that the empirical CDF for the confluences is larger with $p \approx 0.01$ above the PT, while for the knickpoints below the PT we could not reject the null hypothesis with 95% confidence that they belong to the same distribution.

The greater proportions of knickpoints and total knickpoint relief in the tributaries that drain into more glaciated channels support our conceptual model, wherein GLOF erosion can create knickpoints in tributaries at their confluences with the path

Deleted: an

Deleted: that

Deleted:

Deleted: 5970

Deleted: confluences (n = 3062) between

Deleted: and 4th

Deleted: 4th

Deleted: creates knickpoints in tributaries at their confluences with the path of repeated outburst floods. These tributary knickpoints may stall at the confluences (Crosby et al., 2007; Goode and Burbank, 2009),

of repeated outburst floods. These tributary knickpoints may stall at the confluences (Crosby et al., 2007; Goode and Burbank, 2009), or they may propagate upstream. By identifying knickpoints found up to 2 kilometres upstream from a potential GLOF path, we include both possibilities. We limited our analysis to the first 2 kilometres along the tributaries to minimize the possibility of crossing structural or lithologic gradients, which would risk the inclusion of knickpoints formed by other conditions. Another point of interest in our knickpoint inventory is the difference between the distributions of knickpoints with respect to upstream glaciation between rivers above and below the physiographic transition (PT) (Figure 1). Only above the PT do we find a statistically significant offset between the distribution of knickpoints vs. tributaries with increasing glaciated drainage area. This offset is not observed below the PT (Figure 4C).

3.3 Valley widths and the role of GLOFs in "clearing the pipeline" of sediment

We expect that variation in valley floor width reflects the extent of alluviation. Wider valleys should have less frequent bedrock exposure, reflecting aggradation and slower incision. Valleys on GLOF paths should be systemically narrower than expected for a given discharge if GLOFs are clearing out sediment and driving rapid incision frequently enough to control river morphology. As described in the Methods, we measured the widths of valley floors and calculated a normalized wideness index, k_{wn}^*, adjusted for the expected power law increase in channel width with discharge incorporating a discharge estimation to account for the considerable variation in precipitation throughout the study area (Allen et al., 2013; see Methods).

Measurements of valley width corroborate our inferences from k_{sn} and knickpoint occurrence: we find distinct trends in the relationship between valley width and discharge, with rivers that have upstream glaciers being narrower at lower discharges than rivers without glaciated headwaters (Figure 5A). Moreover, among rivers that do include glaciated terrain, valleys with more glaciated drainage area tend to have lower k_{wn} (Figure 5D). These observations suggest that GLOFs keep valley bottoms free of coarse sediment that broadens valleys and armors the bedrock channel bed against erosion. In other words, more frequent GLOFs "clear the pipeline", preventing clogging and allowing valleys to remain narrow. This is not simply a binary relationship, i.e., we do not see valleys with upstream glaciers relatively free of alluvium versus those without glaciers containing substantial fill, but rather find that the valley width appears to depend on the frequency or magnitude of the floods as inferred from upstream glaciated area (Figure 5D).

Deleted: limit

Deleted: risking the inclusion of knickpoints formed by other conditions.

Deleted: ¶
Interestingly, in both k_{sn}^* ratios and knickpoint prevalence, we observe a threshold for the formation of these features. Around 10 km^2 of glaciated drainage area is required before the k_{sn}^* ratios begin to increase (Figure 3). Similarly, knickpoint prevalence only increases where the trunk stream drains on the order of 10 km^2 of above-ELA terrain, although data are relatively scarce for lower areas (only 364 of 5970 knickpoints and 185 of 3062 tributary channels drain to trunk streams with between 1-10^7 m^2 of above-ELA terrain in their basins). Considering the apparent threshold in both metrics, we speculate that an upstream area of glaciated terrain on the order of 10 km^2 is required to produce recognizable outburst flood topography downstream in this region.¶

Deleted: We

Deleted: the same

Deleted: as

Deleted: k_{sn}^*

Deleted: *

Deleted: *

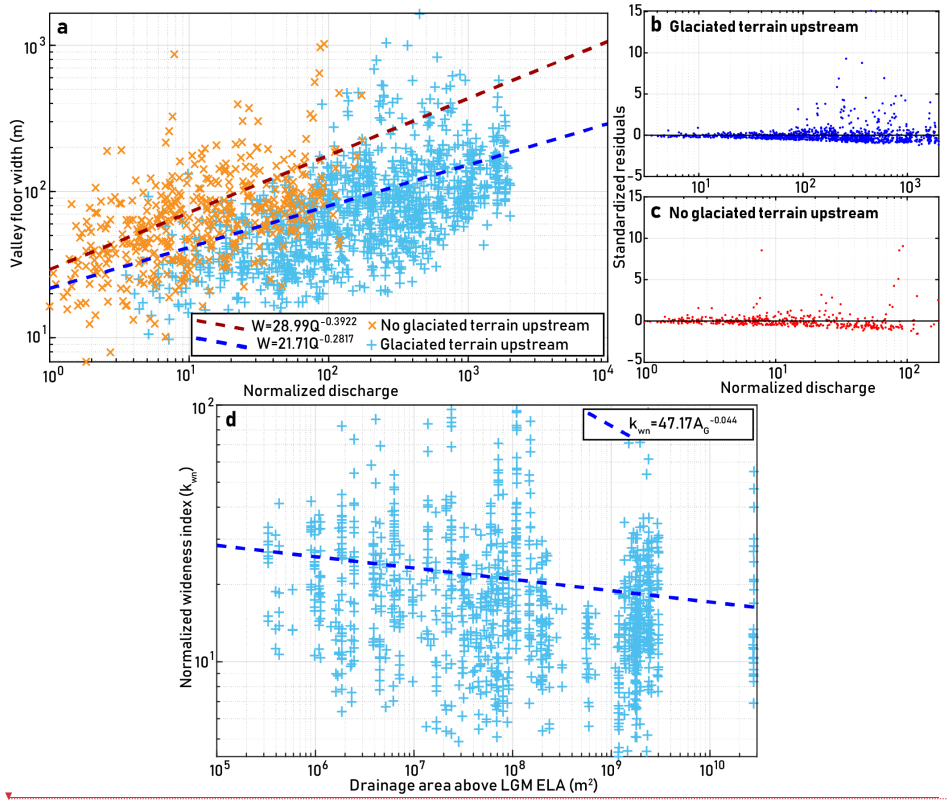

Deleted:

Figure 5 (a) Valley floor width versus discharge for rivers with and without headwaters above the LGM ELA, with power-law fits for valley wideness. Locations of valley width measurements are shown in Supplemental Figure 1. (b-c) Residuals plots for power-law fits shown in Figure 5A. (d) Normalized wideness (k_{wn}) versus contributing drainage area above the LGM ELA for valley width measurements in blue from Figure 5A. Here, A_G refers to drainage area above the ELA. Spearman's ρ = -0.2116 with $P < 0.0001$. We conducted a two-sample Kolmogorov-Smirnov test for the distributions of k_{wn} ratios with above-ELA drainage areas between 10^7-10^8 m^2 (n = 332) and 10^9-10^{10} m^2 (n=378) and found the empirical CDF for the latter group is larger with $P < 0.0001$. Fits shown here were calculated using the "nlinfit" function in Matlab.

Deleted: *)

Deleted: *

3.4 Influence of uplift and erosion on geomorphic metrics

Several other differences across the central Himalaya of Nepal are expected to influence river valley morphology, most notably the pronounced south-to-north increase in uplift and denudation rates. Most of the differences we document as being related to GLOF activity are between different N-S trending river valleys, i.e., between rivers with glaciated headwater versus those without, so we do not expect that differences in uplift and erosion rates are a major confounding factor in our analysis. Nonetheless, to test whether and how differences in uplift and erosion might have complicated our analysis, we examined a subset of basins in the study area which have published estimates of uplift rate derived from river profile analysis (Lavé and Avouac, 2001) and Beryllium-10-derived basin-averaged denudation rates (Godard et al., 2014). These basins contain no or minimal drainage area above the LGM ELA, ruling out the possibility of GLOFs as an important erosion mechanism within these basins and thus allowing us to test for the role of other factors. These basins vary by more than an order of magnitude in uplift and erosion rates, capturing much of the variation found in our study area as a whole (Supplementary Table 1).

For the basins shown in Figure 6, we examined the deviation in k_{sn} deviation from that expected in tributaries to the main drainage, applying the same methods as we used for the whole study area. Figure 7 shows k_{sn} difference from expected plotted against uplift and denudation rates. We found no relationship between denudation or uplift rate and tributary k_{sn}.

We also took additional valley floor width measurements in the studied basins to test for the effect of denudation and uplift rates on valley width versus discharge trends. We fit width-discharge trends for all basins using Equation 6 (results shown in Figure 8). We calculated k_{wn}^* for each basin, using a best-fit b_{ref} of 0.3195. We found no correlation between width-discharge trends and uplift and erosion rates.

Altogether, we observe no coherent relationships between between tributary k_{sn} or basin k_{wn}^* values and either uplift or denudation rate, suggesting that variations in these factors across the study region are not likely to explain the correlations we observe between our metrics of river morphology and the extent of glaciated headwater area. While our analysis based on spatial correlations cannot conclusively rule out other complicating lithologic, tectonic, and climatic factors, we have no reason to expect these to produce the trends we observe.

Deleted: Nonetheless, to test whether and how differences in uplift and erosion might affect the metrics we have used, we examined a subset of basins in the study area which have published estimates of uplift rate derived from river profile analysis (Lavé and Avouac, 2001) and beryllium-10-derived basin-averaged denudation rates (Godard et al., 2014).

Deleted: * ratios between

Deleted: and trunk streams by

Deleted: * ratios at confluences

Deleted: find

Deleted: rate and k_{sn}^* ratios. While there is a weak association between basin

Deleted: k_{sn}^* ratios ($P < 0.05$), our interpretation is that this is unlikely to account for the trend we observe in our results shown in Figure 3.

Deleted: *

Deleted: , allowing us to rule out these factors as major complications for our interpretations

Deleted: * ratios

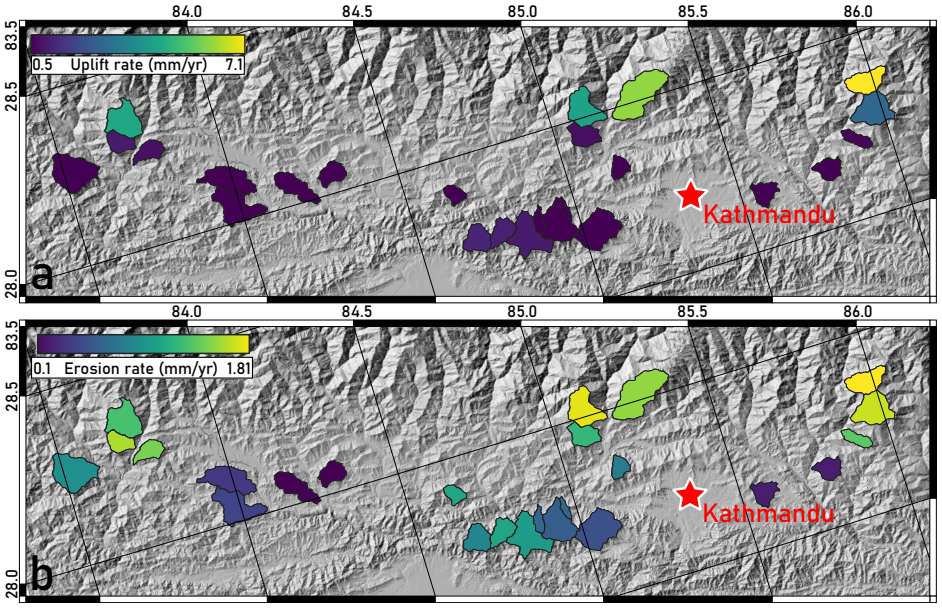

Figure 6 (a) Estimated uplift rate for basins with no or minimal drainage area above the LGM ELA (Lavé and Avouac, 2001). (b) Beryllium-10-derived basin-averaged denudation rates for the same basins (Godard et al., 2014).

Deleted: Figure 6 (a) Estimated uplift rate for basins with no or minimal drainage area above the LGM ELA (Lavé and Avouac, 2001). (b) Beryllium-10-derived basin-averaged denudation rates for the same basins (Godard et al., 2014).¶

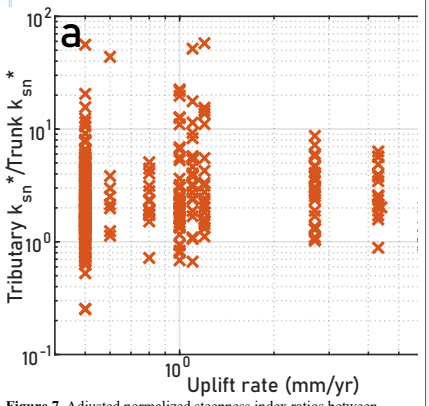

Figure 7. Adjusted normalized steepness index ratios between tributaries and trunk streams vs. uplift and denudation rates in basins identified in Figure 6 (a) k_{sn}^* ratios between tributaries and trunk streams measured at confluences versus uplift rates shown in Figure 6 (Lavé and Avouac, 2001). Spearman's $\rho = 0.1051$ with $P = 0.0384$. (b) Same k_{sn}^* ratios against Beryllium-10-derived denudation rates (Godard et al., 2014). Spearman's $\rho = 0.0650$ with $P = 0.2017$.¶

... [3]

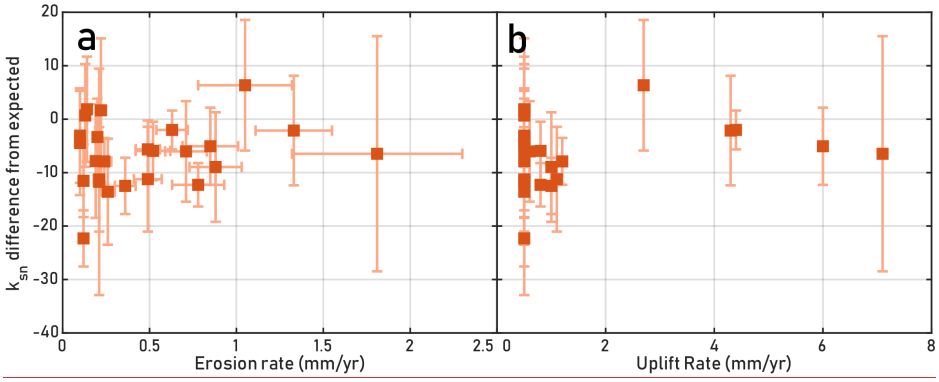

Figure 7. Difference from expected normalized steepness index in tributaries within basins shown in Figure 6 vs. erosion and uplift rates. Expected k_{sn} at tributary elevation was calculated based on same spline fit shown in Figure 3. (a) k_{sn} difference from expected in tributaries versus Beryllium-10-derived denudation rates (Godard et al., 2014). Spearman's $\rho = -0.0306$ with $p = 0.5167$. Vertical errorbars represent 1 standard deviation among tributary k_{sn} values for each basin analyzed. Horizontal were reported from Godard et al. (2014). (b) Same k_{sn} difference from expected in tributaries versus uplift rates (Lavé and Avouac, 2001). Spearman's $\rho = -0.0088$ with $p = 0.8522$.

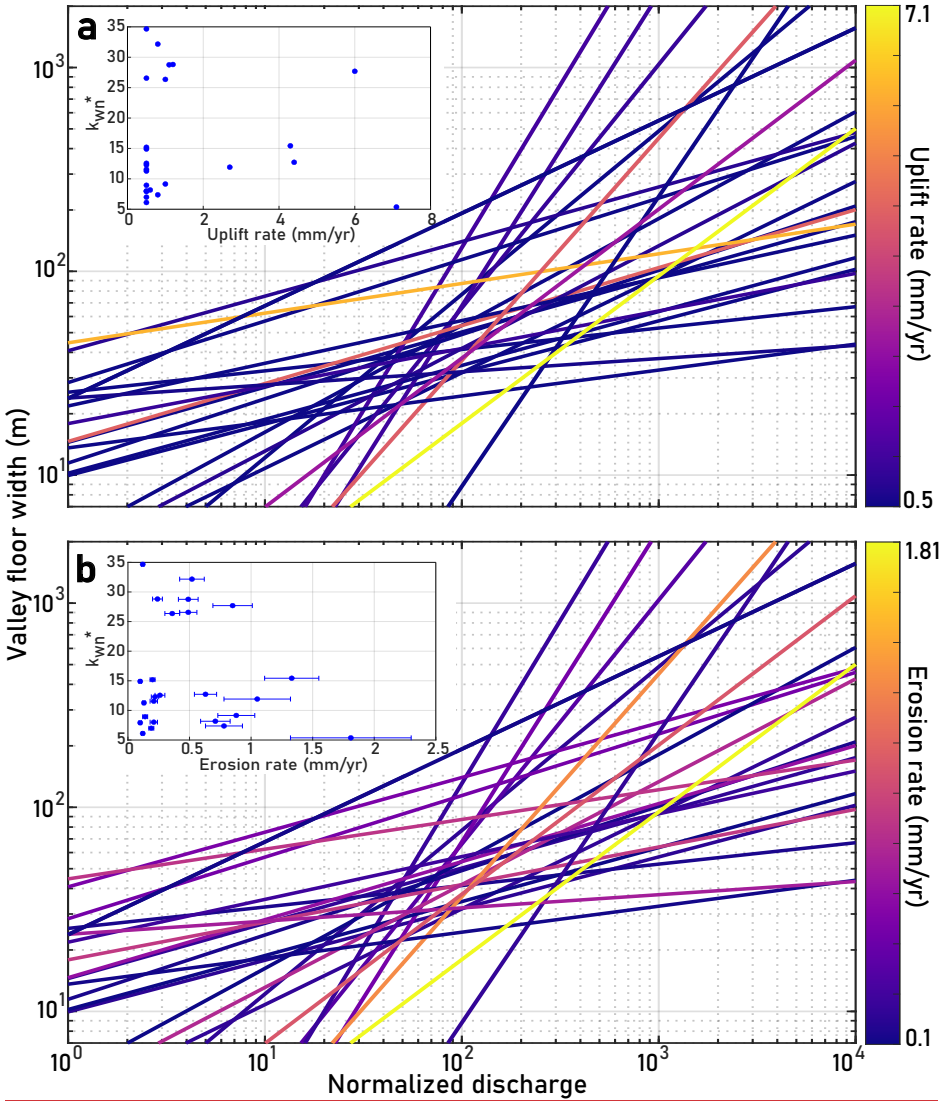
a
b
Valley floor width (m)
Normalized discharge
Uplift rate (mm/yr)
Erosion rate (mm/yr)
k_{wn}^*
7.1
0.5
1.81
0.1

Figure 8 Best-fit lines for valley floor width vs. discharge for basins shown in Figure 6. (a) Lines show best-fit solutions for k_w and b in Equation 6 and are colored by estimated uplift rate for the basin (Lavé and Avouac, 2001). Spearman's ρ = 0.2614 with $P = 0.2069$ for b vs. uplift rate. **Inset:** k_{wn} versus uplift rate. Spearman's ρ = 0.3257 with $P = 0.3257$. (b) Lines show best-fit solutions for k_w and b in Equation 6 and are colored by Beryllium-10-derived denudation rate for the basin (Godard et al., 2014). Spearman's ρ = 0.1289 with $P = 0.5390$ for b vs. denudation rate. **Inset:** k_{wn} versus denudation rate. Spearman's ρ = 0.0758 with $P = 0.7187$.

4 Discussion

4.1 The Physiographic Transition: Shift from "top down" to "bottom up" erosion and complicating factors

Altogether, our analysis suggests that rivers in the central Himalaya bear characteristic signatures of erosion by glacial outburst floods, suggesting that these events are an important but largely under-recognized mechanism of regional incision. Yet GLOFs can only be effective so far downstream. Cook et al. (2018) studied two major GLOFs in the Bhote Khosi valley, occurring in 1981 and 2016, and identified the location of rollover points along the downstream river profile where GLOF discharges attenuated to the point that a monsoon flood with the same recurrence would have greater discharge. Through the 20th and into the 21st centuries, the Bhote Khosi river has experienced GLOFs on a roughly 30-year recurrence (Mool, 1995) , suggesting that the events studied by Cook et al. (2018) may be representative of typical GLOF-driven erosion in this watershed. The rollover points lie very near the prominent physiographic transition (PT) that separates the precipitous High Himalaya from the gentler Middle Hills to the south (Figure 1). The abruptness of the PT reflects the topographic response to a steep gradient in uplift rate and is associated with a pronounced increase in erosion rates from south to north (Burbank et al., 2003; Wobus et al., 2006b; Godard et al., 2014). Over much of its length, the PT also represents a contact between the low-grade Lesser Himalayan Sequence and high-grade High Himalayan Sequence. In our study area, the Kathmandu Nappe juxtaposes High Himalayan rocks into the Lesser Himalaya physiographic region, with no obvious effect on the local topography (Gansser, 1964), although lithology probably plays some role in controlling the PT. In many regions, lithology is an important control on landsliding and thus the formation of landslide-dammed lakes, and on the rate of breakdown of coarse sediment in channels by fluvial action, an alternative mechanism for the mobilization of coarse sediment without necessitating outburst floods. (Sternberg 1875; Gerrard, 1994; Sklar and Dietrich, 2001; Dingle et al., 2017). However, for landslides triggered by the 2015 Gorkha Earthquake, Roback et al. (2018) observed no clear lithologic control, and landslide rates are likely considerably lower in the Middle Hills than the High Himalaya (West et al., 2015).

In this study, we found no significant difference in tributary steepness above and below the PT, though we did identify a subtle increase in potentially GLOF-driven knickpoint generation above the PT (Figure 4). Overall, the influence that GLOFs appear to have on channel steepness, valley width, and knickpoint generation, hint at the possibility of an erosional process domain shift playing a role in the position and nature of major topographic transitions. Specifically, the PT may represent the position

Deleted: (2018)

Deleted: These

Deleted: 1A).¶
¶

Deleted: (Burbank et al., 2003; Wobus et al., 2006b; Godard et al., 2014).

Deleted: , although in

Deleted: substantial effect on the topography (Gansser, 1964). Intriguingly, we find evidence for weakening of the influence of GLOFs on channel geometry when we look at tributary steepness relative to trunk streams above versus below the PT. The relationship between drainage area above the ELA and steepness ratio is no longer evident for confluences below the elevation of the 1981 GLOF rollover point (Figure 3B). These regions of the landscape that are only weakly affected by GLOF erosion would also explain why the highest above-ELA drainage area confluences have anomalously low k_{sn}^* ratios in Figure 3A. It thus appears that the PT may demarcate a shift in erosional process domain, representing the position above which "top-down" GLOF-driven incision is prominent enough to maintain a persistent topographic signature. →

above which "top-down" GLOF-driven incision is prominent enough to maintain a persistent topographic signature. We identified a potential piece of evidence in the knickpoint inventory that hints at a possible supporting role for GLOFs in defining the PT by a process domain transition -- since the extent of upstream glaciation seems to have a role in controlling knickpoint generation above the PT, but less so below it. This interpretation would be consistent with the locations of the rollover points between GLOFs and monsoon floods in the Bhote Khosi.

A shift in process domain could also explain why we do not find distinct relationships between our topographic metrics and rates of uplift or erosion. However, we also recognize that these patterns may be due to the erosional role of landslide lake outburst floods (LLOFs), which can occur almost anywhere in the Himalayan river network, including the Middle Hills, and may be more frequent than GLOFs. For example, in the upper Sutlej River basin, 8 LLOFs occurred since 1973, comparable in peak discharge with the 1981 and 2016 Bhote Koshi floods, and the 2015 Gorkha earthquake triggered ~25,000 landslides forming at least 69 landslide dams (Collins and Jibson, 2015; Ruiz-Villanueva et al., 2017; Roback et al., 2018). If LLOFs are more frequent and widespread, but just as geomorphically effective, the signature of GLOFs may be subtle by comparison, although a top-down erosional regime might still be in force. The distribution of different types of landslide dams in space and time, more varied terrain in which they can occur, and the range of potential magnitudes makes adequate consideration of LLOFs unfeasible in this study (Fan et al., 2020). However, we note that comparison of erosion rates over multiple timescales in this region of the Himalaya suggest a limited role for landslide-driven erosion in the Middle Hills (West et al., 2015) — suggesting that LLOF-driven erosion, like GLOF-driven erosion, may be less pronounced below the PT than above. Nonetheless, we recognize that the interplay of GLOF and LLOF processes is poorly constrained and we hope that this work serves as a starting point for inquiry into their effects as regional agents of erosion. Further complicating the topographic picture is the fact that outburst floods are triggers of landslides along their paths, providing more opportunities for landslide lakes to form and ultimately drain in LLOFs. The interplay of different types of catastrophic floods and their aftermath makes it difficult to isolate the effect of GLOFs independent of other types of outburst flood, we expect that these inter-relationships may be responsible for much of the substantial scatter in our topographic data.

4.2 Implications for development of fluvial hanging valleys

"Fluvial hanging valleys" — steepened tributary reaches near their confluence with mainstem rivers — have been identified previously in the Himalaya and elsewhere. While often considered enigmatic features, their persistence in the landscape has been explained by erosional mechanics that produce lower erosional efficiency in steeper river reaches with low sediment flux (Crosby et al., 2007; Goode and Burbank, 2009). Not all of the steepened zones near confluences that we have identified represent true hanging valley geometry, but our analysis of knickpoint prevalence in tributaries to glaciated rivers may suggest that repeated outburst floods in a trunk stream may, under the correct conditions, control mainstem river incision and generate fluvial hanging valleys. In this case, we explain the formation of these features as resulting from the tributary steepening

Deleted: (Crosby et al., 2007; Goode and Burbank, 2009).

Deleted: analyses

Deleted: both k_{sn}* ratios and

needed to keep pace with the GLOF-driven incision of the mainstem, producing persistent knickpoints near the location where tributaries enter trunk channels with upstream glaciation (Figures 2D-E). We thus propose a connection between the formation of fluvial hanging valleys and upstream glaciation that leads to GLOF-driven erosion in the mainstem. Though the difference in knickpoint distribution that we observe associated with inferred GLOF activity is small, we expect many GLOF-associated tributary knickpoints to be smaller than would be picked up by the 10-meter DEM we have used. Future work might target analyses with higher resolution topographic data, perhaps over smaller areas, to investigate smaller features.

4.3 Landscape Evolution from the Top Down

A simple end-member model of fluvial incision involves the formation of a knickpoint, or localized steepening, in response to uplift which manifests as a drop in a river's base level (Whipple and Tucker, 1999) (Figures 2A-C). In this model, increased steepness causes localized increases in erosion, and the knickpoint propagates upstream. Complexity in this process of incision and knickpoint propagation has been increasingly recognized: channels dominated by bedload abrasion may have knickpoint retreat rates that are decoupled from overall incision rates (Jansen et al., 2011; Wilson et al., 2013), and knickpoints may be smoothed out over years to decades in the presence of copious bedload and sufficient discharge (Cook et al., 2013).

Deleted: (Whipple and Tucker, 1999) (Figures 2A-C).

Deleted: (Jansen et al., 2011; Wilson et al., 2013),

Deleted: (Cook et al., 2013).

Our analysis of Himalayan river channels suggests that "top down" incision driven by GLOFs may be another important factor in driving erosion and determining channel morphology in glaciated mountain belts. Based on relationships we have documented between the area of glaciated headwaters, tributary channel steepness, knickpoint occurrence, and valley widths, we propose that incision processes in the High Himalayan rivers of central Nepal are influenced in important ways from above, by outburst floods from the headwaters of the trunk streams. A critical controlling factor for the geometry of tributaries is their steepening in response to GLOF erosion.

If this process is as pervasive elsewhere as our data suggest it is in the central Himalaya, it would have significant implications for the evolution of orogens in response to tectonic and climatic forcing. In particular, an important role for GLOF erosion, such as that we have identified, implies that the relationship between tectonics and erosion may be modulated by the migration of the ELA. If uplift pushes terrain above the ELA, it could create new glaciers and glacial lakes that, in turn, accelerate GLOF-driven incision. This feedback, in tandem with the propagation of knickpoints from below, could link uplift and erosion rates in ways not captured in current models of landscape evolution. Alongside the effect of tectonics, climatic shifts can drive the ELA to higher or lower elevations, shifting dominant process domains and their signature relief structures to higher or lower elevations. Studies of landscape evolution and interpretations of river channel morphology and network geometry in mountainous environments should consider the influence of outburst floods as regional drivers of erosion, even where glaciers are no longer present. Altogether, our results suggest a rethinking is warranted of classic models of mountain river system evolution, to consider the role of glacial outburst floods as regional controls on erosion.

5 Conclusions

We found several lines of topographic evidence consistent with GLOF-controlled incision in rivers with glaciated headwaters in the Nepal Himalaya. Tributaries to GLOF-prone rivers are steeper than tributaries to non-glaciated rivers, and increasing extent of upstream glaciation in the trunk stream (and thus increasing GLOF frequency) increases this effect. We also found that the knickpoints are more numerous on tributaries to trunk streams with more glaciated terrain upstream, which provides further evidence for the steepening response that highly efficiently eroding outburst flood-dominated channels stimulate in their tributaries.

Additionally, rivers with glaciated headwaters have systematically narrower valleys than unglaciated rivers, indicating that GLOFs effectively sweep coarse alluvium from valleys and expose bedrock to erosion. This effect is increasingly prominent with more upstream glaciation. Alongside previously reported evidence that outburst floods alone can mobilize the large boulders that frequently armor channels in major Himalayan rivers, the regional topographic analysis presented here suggests that GLOFs and other outburst floods, such as landslide lake outburst floods, may be a key erosional mechanism in these rivers. Our results point to a top-down model for valley incision in the Himalaya, in which erosion may be coupled to tectonics by uplift driving terrain above the ELA, expanding the reach of GLOFs, as opposed to (or in addition to) tectonically generated knickpoints propagating throughout Himalayan catchments from base level. GLOF-driven erosion may be important in other glaciated mountain ranges, appears to be independent of uplift and erosion rates, and should be considered in erosion models for such landscapes.

Deleted: form fluvial hanging valleys where

Deleted: is manifest as increased steepness in the tributaries.

Deleted: stream

Deleted: evidences

Deleted: this evidence

Deleted: dominant

Deleted: is

Data Availability

Upon publication, the datasets generated and analysed during the current study will be made available in the Hydroshare repository, http://www.hydroshare.org/resource/2883cfeebb3a43f2b9a1b222e2cfff29

Author Contribution Statement

MPD and AJW conceived the study. MPD performed the analyses. MPD and AJW wrote the manuscript.

Competing Interests

The authors declare that they have no conflict of interest.

Acknowledgments

We thank Kristen Cook, Jens Turowski, Georg Veh, and Missy Eppes for helpful discussions. We also thank William Medwedeff for the photograph used in Figure 2. John Jansen and an anonymous reviewer contributed insightful comments that greatly improved this paper. Geospatial support for this work provided by the Polar Geospatial Center under NSF-OPP awards 1043681 and 1559691. This work was supported by NSF award EAR-1640894.

References

Allen, G. H., Barnes, J. B., Pavelsky, T. M., and Kirby, E.: Lithologic and tectonic controls on bedrock channel form at the northwest Himalayan front, Journal of Geophysical Research: Earth Surface, 118, 1806–1825, https://doi.org/10.1002/jgrf.20113, 2013.

Asahi, K.: Equilibrium-line altitudes of the present and Last Glacial Maximum in the eastern Nepal Himalayas and their implications for SW monsoon climate, Quaternary International, 212, 26–34, https://doi.org/10.1016/j.quaint.2008.08.004, 2010.

Baynes, E. R. C., Attal, M., Niedermann, S., Kirstein, L. A., Dugmore, A. J., and Naylor, M.: Erosion during extreme flood events dominates Holocene canyon evolution in northeast Iceland, Proceedings of the National Academy of Sciences, 112, 2355–2360, https://doi.org/10.1073/pnas.1415443112, 2015.

Bookhagen, B.: High Resolution Spatiotemporal Distribution of Rainfall Seasonality and Extreme Events Based on a 12-year TRMM Time Series, 2013.

Brozović, N., Burbank, D. W., and Meigs, A. J.: Climatic Limits on Landscape Development in the Northwestern Himalaya, Science, 276, 571, https://doi.org/10.1126/science.276.5312.571, 1997.

Burbank, D. W., Blythe, A. E., Putkonen, J., Pratt-Sitaula, B., Gabet, E., Oskin, M., Barros, A., and Ojha, T. P.: Decoupling of erosion and precipitation in the Himalayas, Nature, 426, 652–655, https://doi.org/10.1038/nature02187, 2003.

Cenderelli, D. A. and Wohl, E. E.: Flow hydraulics and geomorphic effects of glacial-lake outburst floods in the Mount Everest region, Nepal, Earth Surface Processes and Landforms, 28, 385–407, https://doi.org/10.1002/esp.448, 2003.

Collins, B. D. and Jibson, R. W.: Assessment of Existing and Potential Landslide Hazards Resulting from the April 25, 2015 Gorkha, Nepal Earthquake Sequence, USGS Open-File Report, 2015.

Cook, K. L., Turowski, J. M., and Hovius, N.: A demonstration of the importance of bedload transport for fluvial bedrock erosion and knickpoint propagation, Earth Surface Processes and Landforms, 38, 683–695, https://doi.org/10.1002/esp.3313, 2013.

Cook, K. L., Andermann, C., Gimbert, F., Adhikari, B. R., and Hovius, N.: Glacial lake outburst floods as drivers of fluvial erosion in the Himalaya, Science, 362, 6410, 53-57, https://doi.org/10.1126/science.aat4981, 2018.

Deleted: John Jansen,

Formatted: Font: Not Bold

Deleted: Allen, G. H., Barnes, J. B., Pavelsky, T. M., and Kirby, E.: Lithologic and tectonic controls on bedrock channel form at the northwest Himalayan front, Journal of Geophysical Research: Earth Surface, 118, 1806–1825, https://doi.org/10.1002/jgrf.20113, 2013.¶
Asahi, K.: Equilibrium-line altitudes of the present and Last Glacial Maximum in the eastern Nepal Himalayas and their implications for SW monsoon climate, Quaternary International, 212, 26–34, https://doi.org/10.1016/j.quaint.2008.08.004, 2010.¶
Baynes, E. R. C., Attal, M., Niedermann, S., Kirstein, L. A., Dugmore, A. J., and Naylor, M.: Erosion during extreme flood events dominates Holocene canyon evolution in northeast Iceland, Proceedings of the National Academy of Sciences, 112, 2355–2360, https://doi.org/10.1073/pnas.1415443112, 2015.¶
Bookhagen, B.: High Resolution Spatiotemporal Distribution of Rainfall Seasonality and → Extreme Events Based on a 12-year TRMM Time Series, 2013.¶
Brozović, N., Burbank, D. W., and Meigs, A. J.: Climatic Limits on Landscape Development in the Northwestern Himalaya, Science, 276, 571, https://doi.org/10.1126/science.276.5312.571, 1997.¶
Burbank, D. W., Blythe, A. E., Putkonen, J., Pratt-Sitaula, B., Gabet, E., Oskin, M., Barros, A., and Ojha, T. P.: Decoupling of erosion and precipitation in the Himalayas, Nature, 426, 652–655, https://doi.org/10.1038/nature02187, 2003.¶
Cenderelli, D. A. and Wohl, E. E.: Flow hydraulics and geomorphic effects of glacial-lake outburst floods in the Mount Everest region, Nepal, Earth Surface Processes and Landforms, 28, 385–407, https://doi.org/10.1002/esp.448, 2003.¶
Cook, K. L., Turowski, J. M., and Hovius, N.: A demonstration of the importance of bedload transport for fluvial bedrock erosion and knickpoint propagation, Earth Surface Processes and Landforms, 38, 683–695, https://doi.org/10.1002/esp.3313, 2013.¶
Cook, K. L., Andermann, C., Gimbert, F., Adhikari, B. R., and Hovius, N.: Glacial lake outburst floods as drivers of fluvial erosion in the Himalaya, Science, 362, 6410, 53-57, https://doi.org/10.1126/science.aat4981, 2018.¶
Croissant, T., Lague, D., Steer, P., and Davy, P.: Rapid post-seismic landslide evacuation boosted by dynamic river width, Nature Geoscience, 10, 680–684, https://doi.org/10.1038/ngeo3005, 2017.¶
Crosby, B. T., Whipple, K. X., Gasparini, N. M., and Wobus, C. W.: Formation of fluvial hanging valleys: Theory and simulation, Journal of Geophysical Research, 112, https://doi.org/10.1029/2006JF000566, 2007.¶
Cunningham, M. T., Stark, C. P., Kaplan, M. R., and Schaefer, J. M.: Glacial limitation of tropical mountain height, Earth Surface Dynamics, 7, 147–169, https://doi.org/10.5194/esurf-7-147-2019, 2019.¶
Dahlquist, M. P. and West, A. J.: Initiation and Runout of Post-Seismic Debris Flows: Insights From the 2015 Gorkha Earthquake, Geophysical Research Letters, 46, 9658–9668, https://doi.org/10.1029/2019GL083548, 2019.¶
Davis, William Morris: Glacial Erosion in France, Switzerland and Norway, Proceedings of the Boston Society of Natural History, 29, 273–321, 1900.¶
DiBiase, R. A. and Whipple, K. X.: The influence of erosion thresholds and runoff variability on the relationships among topography, climate, and erosion rate, Journal of Geophysical Research, 116, https://doi.org/10.1029/2011JF002095, 2011.¶
Egholm, D. L., Nielsen, S. B., Pedersen, V. K., and Lesemann, J.-E.: Glacial effects limiting mountain height, Nature, 460, 884–887, https://doi.org/10.1038/nature08263, 2009.¶

... [4]

Croissant, T., Lague, D., Steer, P., and Davy, P.: Rapid post-seismic landslide evacuation boosted by dynamic river width, 10, 680–684, https://doi.org/10.1038/ngeo3005, Nature Geoscience, 2017.

Crosby, B. T., and Whipple, K. X.: Knickpoint initiation and distribution within fluvial networks: 236 waterfalls in the Waipaoa River, North Island, New Zealand, Geomorphology, 82, 1-2, 16-38, https://doi.org/10.1016/j.geomorph.2005.08.023, 2006.

Crosby, B. T., Whipple, K. X., Gasparini, N. M., and Wobus, C. W.: Formation of fluvial hanging valleys: Theory and simulation, Journal of Geophysical Research, 112, https://doi.org/10.1029/2006JF000566, 2007.

Cunningham, M. T., Stark, C. P., Kaplan, M. R., and Schaefer, J. M.: Glacial limitation of tropical mountain height, Earth Surface Dynamics, 7, 147–169, https://doi.org/10.5194/esurf-7-147-2019, 2019.

Dahlquist, M. P. and West, A. J.: Initiation and Runout of Post-Seismic Debris Flows: Insights From the 2015 Gorkha Earthquake, Geophysical Research Letters, 46, 9658–9668, https://doi.org/10.1029/2019GL083548, 2019.

Davis, William Morris: Glacial Erosion in France, Switzerland and Norway, Proceedings of the Boston Society of Natural History, 29, 273–321, 1900.

DiBiase, R. A. and Whipple, K. X.: The influence of erosion thresholds and runoff variability on the relationships among topography, climate, and erosion rate, Journal of Geophysical Research, 116, https://doi.org/10.1029/2011JF002095, 2011.

Dingle, E. H., Attal, M., and Sinclair, H. D.: Abrasion-set limits on Himalayan gravel flux, Nature, 544, 471–474, https://doi.org/10.1038/nature22039, 2017.

Egholm, D. L., Nielsen, S. B., Pedersen, V. K., and Lesemann, J.-E.: Glacial effects limiting mountain height, Nature, 460, 884–887, https://doi.org/10.1038/nature08263, 2009.

Fan, X., Dufresne, A., Siva Subramanian, S., Strom, A., Hermanns, R., Tacconi Stefanelli, C., Hewitt, K., Yunus, A. P., Dunning, S., Capra, L., Geertsema, M., Miller, B., Casagli, N., Jansen, J. D., and Xu, Q.: The formation and impact of landslide dams – State of the art, Earth-Science Reviews, 203, 103116, https://doi.org/10.1016/j.earscirev.2020.103116, 2020.

Finnegan, N. J., Roe, G., Montgomery, D. R., and Hallet, B.: Controls on the channel width of rivers: Implications for modeling fluvial incision of bedrock, Geology, 33, 229, https://doi.org/10.1130/G21171.1, 2005.

Finnegan, N. J., Schumer, R., and Finnegan, S.: A signature of transience in bedrock river incision rates over timescales of 104–107 years, Nature, 505, 391–394, https://doi.org/10.1038/nature12913, 2014.

Fischer, M., Korup, O., Veh, G., and Walz, A.: Controls of outbursts of moraine-dammed lakes in the greater Himalayan region, The Cryosphere, 15, 4145-4163, https://doi.org/10.5194/tc-15-4145-2021, 2021.

Flint, J. J.: Stream gradient as a function of order, magnitude, and discharge, Water Resources Research, 10, 969–973, https://doi.org/10.1029/WR010i005p00969, 1974.

Forte, A. M. and Whipple, K. X.: Short communication: The Topographic Analysis Kit (TAK) for TopoToolbox, Earth Surface Dynamics, 7, 87–95, https://doi.org/10.5194/esurf-7-87-2019, 2019.

Gansser, A.: Geology of the Himalayas, Interscience Publishers, London, 289 pp., 1964.

Gardner, T. W., Jorgensen, D. W., Shuman, C., and Lemieux, C., R.: Geomorphic and tectonic process rates: Effects of measured time interval, Geology, 15, 259–261, 1987.

Gerrard, J.: The landslide hazard in the Himalayas: geological control and human action, Geomorphology, 10, 221-230, 1994.

Godard, V., Bourles, D. L., Spinabella, F., Burbank, D. W., Bookhagen, B., Fisher, G. B., Moulin, A., and Leanni, L.: Dominance of tectonics over climate in Himalayan denudation, Geology, 42, 243–246, https://doi.org/10.1130/G35342.1, 2014.

Goode, J. K. and Burbank, D. W.: Numerical study of degradation of fluvial hanging valleys due to climate change, Journal of Geophysical Research, 114, https://doi.org/10.1029/2007JF000965, 2009.

Haeberli, Wilfried: Frequency and Characteristics of Glacier Floods in the Swiss Alps, Annals of Glaciology, 4, 85–90, https://doi.org/10.3189/S0260305500005280, 1983.

Hewitt, K.: Catastrophic landslides and their effects on the Upper Indus streams, Karakoram Himalaya, northern Pakistan, Geomorphology, 26, 47–80, https://doi.org/10.1016/S0169-555X(98)00051-8, 1998.

Hilton, R. G. and West, A. J.: Mountains, erosion and the carbon cycle, Nature Reviews Earth & Environment, 1, 284–299, https://doi.org/10.1038/s43017-020-0058-6, 2020.

Howard, A. D.: A detachment-limited model of drainage basin evolution, Water Resources Research, 30, 2261–2285, https://doi.org/10.1029/94WR00757, 1994.

Huber, M. L., Lupker, M., Gallen, S. F., Christl, M., and Gajurel, A. P.: Timing of exotic, far-travelled boulder emplacement and paleo-outburst flooding in the central Himalaya, Earth Surface Dynamics, 8, 769-787, https://doi.org/10.5194/esurf-8-769-2020, 2020.

Jacquet, J., McCoy, S. W., McGrath, D., Nimick, D. A., Fahey, M., O'kuinghttons, J., Friesen, B. A., and Leidich, J.: Hydrologic and geomorphic changes resulting from episodic glacial lake outburst floods: Rio Colonia, Patagonia, Chile, Geophysical Research Letters, 44, 854–864, https://doi.org/10.1002/2016GL071374, 2017.

Jansen, J. D., Fabel, D., Bishop, P., Xu, S., Schnabel, C., and Codilean, A. T.: Does decreasing paraglacial sediment supply slow knickpoint retreat?, Geology, 39, 543–546, https://doi.org/10.1130/G32018.1, 2011.

Kirby, E. and Whipple, K.: Quantifying differential rock-uplift rates via stream profile analysis, Geology, 29, 415, https://doi.org/10.1130/0091-7613(2001)029<0415:QDRURV>2.0.CO;2, 2001.

Kirchner, J. W., Finkel, R. C., Riebe, C. S., Granger, D. E., Clayton, J. L., King, J. G., and Megahan, W. F.: Mountain erosion over 10 yr, 10 k.y., and 10 m.y. time scales, Geology, 29, 591, https://doi.org/10.1130/0091-7613(2001)029<0591:MEOYKY>2.0.CO;2, 2001.

Kirchner, N., Greve, R., Stroeven, A. P., and Heyman, J.: Paleoglaciological reconstructions for the Tibetan Plateau during the last glacial cycle: evaluating numerical ice sheet simulations driven by GCM-ensembles, Quaternary Science Reviews, 30, 248–267, https://doi.org/10.1016/j.quascirev.2010.11.006, 2011.

Korup, O. and Tweed, F.: Ice, moraine, and landslide dams in mountainous terrain, Quaternary Science Reviews, 26, 3406–3422, https://doi.org/10.1016/j.quascirev.2007.10.012, 2007.

Korup, O., Montgomery, D. R., and Hewitt, K.: Glacier and landslide feedbacks to topographic relief in the Himalayan syntaxes, 107, 5317–5322, Proceedings of the National Academy of Sciences, https://doi.org/10.1073/pnas.0907531107, 2010.

Lague, D., Hovius, N., and Davy, P.: Discharge, discharge variability, and the bedrock channel profile, Journal of Geophysical Research: Earth Surface, 110, F4, https://doi.org/10.1029/2004JF000259, 2005.

Lang, K. A., Huntington, K. W., and Montgomery, D. R.: Erosion of the Tsangpo Gorge by megafloods, Eastern Himalaya, Geology, 41, 1003–1006, https://doi.org/10.1130/G34693.1, 2013.

Larsen, I. J. and Montgomery, D. R.: Landslide erosion coupled to tectonics and river incision, Nature Geoscience, 5, 468–473, https://doi.org/10.1038/ngeo1479, 2012.

Lavé, J. and Avouac, J. P.: Fluvial incision and tectonic uplift across the Himalayas of central Nepal, Journal of Geophysical Research: Solid Earth, 106, 26561–26591, https://doi.org/10.1029/2001JB000359, 2001.

Leopold, L. B. and Maddock, T.: The Hydraulic Geometry of Stream Channels and Some Physiographic Implications, United States Geological Survey Professional Paper 252, 1953.

Lutz, A. F., Immerzeel, W. W., Shrestha, A. B., and Bierkens, M. F. P.: Consistent increase in High Asia's runoff due to increasing glacier melt and precipitation, Nature Climate Change, 4, 587–592, https://doi.org/10.1038/nclimate2237, 2014.

Martens, B., Miralles, D. G., Lievens, H., van der Schalie, R., de Jeu, R. A. M., Fernández-Prieto, D., Beck, H. E., Dorigo, W. A., and Verhoest, N. E. C.: GLEAM v3: satellite-based land evaporation and root-zone soil moisture, Geoscientific Model Development, 10, 1903–1925, https://doi.org/10.5194/gmd-10-1903-2017, 2017.

Mason, Kenneth: Indus floods and Shyok glaciers, The Himalayan Journal, 1, 10–29, 1929.

Massey, F. J.: The Kolmogorov-Smirnov Test for Goodness of Fit, Journal of the American Statistical Association, 46, 68–78, 1951.

Montgomery, D. R. and Foufoula-Georgiou, E.: Channel network source representation using digital elevation models, Water Resources Research, 29, 3925–3934, https://doi.org/10.1029/93WR02463, 1993.

Montgomery, D. R., Hallet, B., Yuping, L., Finnegan, N., Anders, A., Gillespie, A., and Greenberg, H. M.: Evidence for Holocene megafloods down the Tsangpo River gorge, Southeastern Tibet, Quaternary Research, 62, 201–207, https://doi.org/10.1016/j.yqres.2004.06.008, 2004.

Mool, P.K.: Glacier Lake Outburst Floods in Nepal, Journal of Nepal Geological Society, 11, 273–280. https://doi.org/10.3126/jngs.v11i0.32802, 1995.

Pickering, J. L., Diamond, M. S., Goodbred, S. L., Grall, C., Martin, J. M., Palamenghi, L., Paola, C., Schwenk, T., Sincavage, R. S., and Spieß, V.: Impact of glacial-lake paleofloods on valley development since glacial termination II: A conundrum of hydrology and scale for the lowstand Brahmaputra-Jamuna paleovalley system, Geological Society of America Bulletin, 131, 58–70, https://doi.org/10.1130/B31941.1, 2019.

Polar Geospatial Center: EarthDEM - Polar Geospatial Center, 2021.

Prasicek, G., Herman, F., Robl, J., and Braun, J.: Glacial Steady State Topography Controlled by the Coupled Influence of Tectonics and Climate, Journal of Geophysical Research: Earth Surface, 123, 1344–1362, https://doi.org/10.1029/2017JF004559, 2018.

Ray, Y. and Srivastava, P.: Widespread aggradation in the mountainous catchment of the Alaknanda–Ganga River System: timescales and implications to Hinterland–foreland relationships, Quaternary Science Reviews, 29, 2238–2260, https://doi.org/10.1016/j.quascirev.2010.05.023, 2010.

Raymo, M. E. and Ruddiman, W. F.: Tectonic forcing of late Cenozoic climate, Nature, 359, 117–122, https://doi.org/10.1038/359117a0, 1992.

Roback, K., Clark, M. K., West, A. J., Zekkos, D., Li, G., Gallen, S. F., Chamlagain, D., and Godt, J. W.: The size, distribution, and mobility of landslides caused by the 2015 M w 7.8 Gorkha earthquake, Nepal, Geomorphology, 301, 121–138, https://doi.org/10.1016/j.geomorph.2017.01.030, 2018.

Roe, G. H., Montgomery, D. R., and Hallet, B.: Orographic precipitation and the relief of mountain ranges, Journal of Geophysical Research: Solid Earth, 108, https://doi.org/10.1029/2001JB001521, 2003.

Ruiz-Villanueva, V., Allen, S., Arora, M., Goel, N. K., and Stoffel, M.: Recent catastrophic landslide lake outburst floods in the Himalayan mountain range, Progress in Physical Geography: Earth and Environment, 41, 3–28, https://doi.org/10.1177/0309133316658614, 2017.

Scherler, D., Munack, H., Mey, J., Eugster, P., Wittmann, H., Codilean, A. T., Kubik, P., and Strecker, M. R.: Ice dams, outburst floods, and glacial incision at the western margin of the Tibetan Plateau: A >100 k.y. chronology from the Shyok Valley, Karakoram, Geological Society of America Bulletin, 126, 738–758, https://doi.org/10.1130/B30942.1, 2014.

Schwanghart, W. and Scherler, D.: Short Communication: TopoToolbox 2 – MATLAB-based software for topographic analysis and modeling in Earth surface sciences, Earth Surface Dynamics, 2, 1–7, https://doi.org/10.5194/esurf-2-1-2014, 2014.

Schwanghart, W., Bernhardt, A., Stolle, A., Hoelzmann, P., Adhikari, B. R., Andermann, C., Tofelde, S., Merchel, S., Rugel, G., Fort, M., and Korup, O.: Repeated catastrophic valley infill following medieval earthquakes in the Nepal Himalaya, Science, 351, 147–150, https://doi.org/10.1126/science.aac9865, 2016.

Shields, A.: Application of similarity principles and turbulence research to bed-load movement, CalTech library, Soil Conservation Service Cooperative Laboratory, California Institute of Technology, Pasadena, California, USA, 1936.

Sklar, L. S. and Dietrich, W. E.: Sediment and rock strength controls on river incision into bedrock, Geology, 29, 1087, https://doi.org/10.1130/0091-7613(2001)029<1087:SARSCO>2.0.CO;2, 2001.

Sklar, L. S. and Dietrich, W. E.: The role of sediment in controlling steady-state bedrock channel slope: Implications of the saltation–abrasion incision model, Geomorphology, 82, 58–83, https://doi.org/10.1016/j.geomorph.2005.08.019, 2006.

Snyder, N. P., Whipple, K. X., Tucker, G. E., and Merritts, D. J.: Importance of a stochastic distribution of floods and erosion thresholds in the bedrock river incision problem, Journal of Geophysical Research: Solid Earth, 108, https://doi.org/10.1029/2001JB001655, 2003.

Spearman, C.: The Proof and Measurement of Association between Two Things, The American Journal of Psychology ,100, 441–471, 1987.

Steer, P., Simoes, M., Cattin, R., and Shyu, J. B. H.: Erosion influences the seismicity of active thrust faults, Nature Communications, 5, 5564, https://doi.org/10.1038/ncomms6564, 2014.

Sternberg, H.: Untersuchungen über längen- und Querprofil geschiebeführender Flüsse, Zeitschrift für Bauwesen, 25, 486–506, 1875.

Stock, J. D. and Dietrich, W. E.: Erosion of steepland valleys by debris flows, Geological Society of America Bulletin, 118, 1125–1148, 2006.

Thomson, S. N., Brandon, M. T., Tomkin, J. H., Reiners, P. W., Vásquez, C., and Wilson, N. J.: Glaciation as a destructive and constructive control on mountain building, Nature, 467, 313–317, https://doi.org/10.1038/nature09365, 2010.

Turowski, J. M., Yager, E. M., Badoux, A., Rickenmann, D., and Molnar, P.: The impact of exceptional events on erosion, bedload transport and channel stability in a step-pool channel, Earth Surface Processes and Landforms, 34, 1661–1673, https://doi.org/10.1002/esp.1855, 2009.

Veh, G., Korup, O., von Specht, S., Roessner, S., and Walz, A.: Unchanged frequency of moraine-dammed glacial lake outburst floods in the Himalaya, Nature Climate Change, 9, 379–383, https://doi.org/10.1038/s41558-019-0437-5, 2019.

Veh, G., Korup, O., and Walz, A.: Hazard from Himalayan glacier lake outburst floods, Proceedings of the National Academy of Sciences, 117, 907–912, https://doi.org/10.1073/pnas.1914898117, 2020.

Whipple, K. X. and Tucker, G. E.: Dynamics of the stream-power river incision model: Implications for height limits of mountain ranges, landscape response timescales, and research needs, Journal of Geophysical Research: Solid Earth, 104, 17661–17674, https://doi.org/10.1029/1999JB900120, 1999.

Whittaker, A. C.: How do landscapes record tectonics and climate?, Lithosphere, 4, 160–164, https://doi.org/10.1130/RF.L003.1, 2012.

Willett, S. D. and Brandon, M. T.: On steady states in mountain belts, Geology, 30, 175, https://doi.org/10.1130/0091-7613(2002)030<0175:OSSIMB>2.0.CO;2, 2002.

Wilson, A., Hovius, N., and Turowski, J. M.: Upstream-facing convex surfaces: Bedrock bedforms produced by fluvial bedload abrasion, Geomorphology, 180–181, 187–204, https://doi.org/10.1016/j.geomorph.2012.10.010, 2013.

Wobus, C., Whipple, K. X., Kirby, E., Snyder, N., Johnson, J., Spyropolou, K., Crosby, B., and Sheehan, D.: Tectonics from topography: Procedures, promise, and pitfalls, in: Special Paper 398: Tectonics, Climate, and Landscape Evolution, vol. 398, Geological Society of America, 55–74, https://doi.org/10.1130/2006.2398(04), 2006a.

Wobus, C. W., Whipple, K. X., and Hodges, K. V.: Neotectonics of the central Nepalese Himalaya: Constraints from geomorphology, detrital ^{40}Ar/^{39}Ar thermochronology, and thermal modeling, Tectonics, 25, https://doi.org/10.1029/2005TC001935, 2006b.

Xu, D.: Characteristics of debris flow caused by outburst of glacial lake in Boqu river, Xizang, China, 1981, GeoJournal, 17, 4, https://doi.org/10.1007/BF00209443, 1988.

Yanites, B. J.: The Dynamics of Channel Slope, Width, and Sediment in Actively Eroding Bedrock River Systems, Journal of Geophysical Research: Earth Surface, 123, 1504–1527, https://doi.org/10.1029/2017JF004405, 2018.

Yanites, B. J., Mitchell, N. A., Bregy, J. C., Carlson, G. A., Cataldo, K., Holahan, M., Johnston, G. H., Nelson, A., Valenza, J., and Wanker, M.: Landslides control the spatial and temporal variation of channel width in southern Taiwan: Implications for landscape evolution and cascading hazards in steep, tectonically active landscapes, Earth Surface Processes and Landforms, 43, 1782–1797, https://doi.org/10.1002/esp.4353, 2018.

1410

Page 2: [1] Deleted	**Maxwell Dahlquist**	**2/15/22 11:45:00 AM**
Page 9: [2] Deleted	**Maxwell Dahlquist**	**2/15/22 11:45:00 AM**
Page 19: [3] Deleted	**Maxwell Dahlquist**	**2/15/22 11:45:00 AM**
Page 26: [4] Deleted	**Maxwell Dahlquist**	**2/15/22 11:45:00 AM**